Relation between structural patterns and magnetism in small iron oxide clusters; reentrance of magnetic moment at high oxidation rates.

R. H. Aguilera-del-Toro,[1] F. Aguilera-Granja,[2] M. B. Torres,[3, *] and A. Vega[1]

[1]*Departamento de Física Teórica, Atómica y Óptica,*

Universidad de Valladolid, E-47011 Valladolid, Spain

[2]*Instituto de Física, Universidad Autónoma de San Luis Potosí, México*

[3]*Departamento de Matemáticas y Computación, Universidad de Burgos, Spain*

(Dated: July 16, 2020)

Abstract

The unavoidable oxidation in environmental conditions leads to the formation of iron oxide nanoparticles that are very interesting from both theoretical and experimental points of view. The biocompatibility of iron oxide clusters makes them outstanding candidates for nanomedicine. Due to quantum confinement effects, the understanding of iron oxide nanoparticles is a challenge that opens the possibility of designing nanomaterials with new capacities. In this work, we report a theoretical density functional theory study of the structural and electronic properties as well as of the magnetic properties of neutral and charged iron oxide clusters $Fe_nO_m^{0/\pm}$ ($n = 1 - 6$), with m values until oxygen saturation is achieved. We determine the putative ground state configuration and low-energy structural and spin isomers. Based on total energy differences between the obtained global minimum structure of parent clusters and their possible fragments, we explore the fragmentation channels for cation oxides comparing with experiments. Our results provide a fundamental insight on how the structural pattern develops upon oxidation and its connection with the magnetic couplings and net total moment. Upon addition of oxygen, electronic charge transfer from iron to oxygen is found which weakens the iron-iron bond and, consequently the direct exchange coupling in Fe. The binding energy increases to reach a plateau for different oxidation rates depending on size, and it does not decrease until the molecular oxygen adsorption starts to take place. The oxygen environment is a crucial factor related to stabilities and to the magnetic character of iron oxides. We identified certain iron oxide clusters of special relevance in the context of magnetic grains due to of their high stability, expected abundance and ferromagnetic-like character that cause large total magnetic moments even at high oxidation rates.

I. INTRODUCTION

Iron oxides are very common and abundant in natural conditions. They are also formed as corrosion products and can be easily synthesized. The unavoidable oxidation in certain environmental conditions facilitates their production. Besides, they are relatively easy to prepare with low cost. Designing nanoparticles that retain a net magnetic moment in realist conditions is challenging. In addition, iron oxide nanoparticles are of great interest from both the fundamental and technological points of view[1]. Since the properties of a material can be drastically modified at the nanoscale due to quantum confinement effects, with non-monotonous dependencies on cluster size, composition, and number of electrons, understanding the physics and chemistry of iron oxide nanoparticles is now a days a great challenge, but at the same time opens the possibility of finding and designing systems with new capabilities. The intrinsic magnetic properties and biocompatibility of iron oxide clusters makes them one of the most suitable candidates for nanomedicine. Those smaller than 30 nm are superparamagnetic at room temperature and can be used for drug delivery[2,3], cancer therapy through magnetic hyperthermia[4], as contrast agents for Magnetic Resonance Imaging (MRI)[5], and the emerging technique of Magnetic Particle Imaging (MPI)[6]. A recent work[7] suggests that prostate tumours with high nerve densities are more likely to grow and spread than those with low nerve densities. Such high-risk cases can be identified using a combination of MRI, magnetic particle imaging (MPI) and functionalized iron-oxide nanoparticles. In experiments with mice, the researchers also used the same nanoparticles to deliver a drug that blocks nerve function, with successful results. You *et al.*[7] developed a contrast agent that targets nervous tissue specifically. The team started with iron oxide nanoparticles, which have already found use in both MRI and MPI, and joined them to the nerve-binding peptide NP41. It is, therefore, not surprising that iron oxide clusters or nanoparticles have been the subject of numerous experimental and theoretical studies during the last years, a representative amount of which are summarized in the following part of the introduction (we apologize if our search was not complete).

Iron oxides FeO_m^- and $Fe_2O_m^-$ ($m = 1 - 4$ and $m = 1 - 5$, respectively) have been studied by anion photoelectron spectroscopy[8] at 3.49 and 4.66 eV photon energies. The vibrational resolved photoelectron spectra and low-lying excited states were obtained. The photoelectron spectra were better resolved for those clusters with a big ratio of oxygen

atoms. Results indicated that the electron affinity of the neutral ones increases with the number of oxygen atoms, suggesting a sequential oxidation behavior. Photoelectron spectra of small anionic iron clusters $Fe_nO_m^-$ (n = 1-4, m =1-6) has been obtained BY Wang et $al.$[9]. They concluded that the oxidation can be viewed as sequential oxygen atom adsorption at the surfaces of the Fe_3 and Fe_4 clusters, leading to a nearly linear increase of the electron affinity with the number of oxygen atoms.

Guided ion beam was used for the study of the reaction of cationic $Fe_n{}^+$ clusters (n = $2-18$) with CO_2[10] and O_2[11] in order to determine the bond energies of those iron clusters with oxide and dioxide; with the former, bond energies are between 3.0 and 6.5 eV, whilst from the second one, bond energies are between 3.6 and 5.15 eV. Cationic iron oxide clusters, $Fe_nO_m{}^+$, were also produced[12] by chemical ionization of $Fe(CO)_5/O_2$ mixtures. They exhibit remarkable fragmentation trends that can be attributed to the formal oxidation states of iron. For clusters with $n/m \geq 1$, the loss of atomic oxygen and FeO units is preferred. For $Fe_nO_m{}^+$ with 1> n/m >2/3, in addition to the loss of O and FeO, loss of neutral FeO_2 was also observed. Finally, for rich oxygen clusters ($n/m = 2/3$), loss of molecular oxygen predominate. Photodissociation of cationic $Fe_nO_m^+$ ($n = 1-15$) clusters was studied by Molek et $al.$[13]. Clusters were produced by laser vaporization in a pulsed nozzle (355 nm) cluster source and detected with Time-Of-Flight (TOF) mass spectrometry. Results indicated that dissociation occurs mainly BY two ways, the first one is the lost of molecular oxygen, and the second is a fission process. For $n \leq 5$, the oxygen elimination process takes place until $m = n$. Then, no more oxygen loss was observed, instead a fission process takes place losing smaller clusters. Iron oxide clusters $Fe_nO_m{}^+$ (n =1-3, m =1-6) have been synthesized in a laser vaporization source and dissociated via CID by Li[14] et $al.$ Examining the dissociation behavior in a wide range of energies, these authors showed that the clusters can be dissociated by evaporation of the Fe and O atoms, as well as the fission of the neutral O_2, FeO, FeO_2, Fe_2O_2 and Fe_2O_3 fragments. In general, they found that the predominant dissociation pathways correlate with the oxidation state of iron in the cluster.

Regarding the theoretical studies, Shiroishi et $al.$[15-16] performed Density Functional Theory (DFT) calculations of Fe_nO_m (n =1-3) and $Fe_nO_m^-$ with ($n = 3, 4$) using first principles molecular dynamics within the Generalized Gradient Approximation (GGA) for the exchange correlation (xc) energy. For all studied clusters, bridge positions were preferred. Magnetic couplings change from ferromagnetic to antiferromagnetic in $m = n$, except for

$Fe_4O_m^-$ in which the change takes place at m =3. Vertical detachment energies were calculated and compared with experimental results[9]. The structural and magnetic properties of $(Fe_2O_3)_n$ (n =1-5) clusters were investigated by Erlebach et $al.$[17], using the TURBOMOLE DFT package, with the B3LYP functional and the Multipole Accelerated Resolution of the Identity (MARI-J) method for the Coulomb term. The results found a good agreement with experimental collision cross sections. A theoretical study of $(FeO)_n^{0/\pm}$ clusters ($n = 1 - 8$) was performed by Ju et $al.$[18] using GAUSSIAN 09 package in the GGA approximation with the PW91 functional and $6-311+G^*$ basis set. Results showed that $(FeO)_4^-$ and $(FeO)_4^+$ clusters have the largest HOMO-LUMO gap values, an indication of their high stability.

Reilly et $al.$[19-20] carried out a combined experimental and theoretical study of the structures and reactivity of $Fe_nO_m^+$ and $Fe_nO_m^-$ ($n = 1 - 2$ and $m = 3 - 5, 6$), respectively, with CO. Clusters were produced by laser vaporization and were characterized by employing a guided ion beam mass spectrometer. Moreover, energy-resolved Collision-Induced Dissociation (CID) experiments were conducted in order to study the fragmentation patterns of those clusters. Theoretical calculations were performed within the DFT-GGA, as implemented in the code deMon2k. Dissociation energies and vertical detachment energies were calculated, with which our results will be compared. Another combined experimental and theoretical study was carried out recently for cationic $Fe_nO_m^+$ ($n = 2 - 6$) clusters by Koyama et $al.$[21]. They performed a theoretical ($n = 4$, $m = 1 - 8$) and experimental ($n = 2 - 6$) study of the dissociation energy for O_2 release. Clusters were formed by laser ablation in a source and selected using mass spectrometry in combination with the post-heating method. A clearly relation between the temperature and the intensity ratios of $Fe_2O_m^+$ was found: as the temperature increase the abundance of the oxygen-rich clusters decreases. Moreover, as the relative abundance of the $Fe_2O_6^+$ clusters decreases, the abundance of $Fe_2O_4^+$ clusters increases, until approximately 550 K; after that, the relative abundance of these clusters decreases, whilst the abundance of $Fe_2O_2^+$ ones increases to the same extent as that of $Fe_2O_6^+$ decreases. Consequently, it was deduced that oxygen is released molecularly in the following form: $Fe_2O_6^+ \rightarrow Fe_2O_4^+ + O_2 \rightarrow Fe_2O_2^+ + 2(O_2)$. To complete the experimental work, theoretical calculations was performed using the GAUSSIAN09 program with the B3LYP functional and 6-311+G* basis set.

In a more general context, Wang et $al.$[22] investigated the structural and magnetic properties of late transition metal oxide clusters, TM$_n$O$_m$ (TM=Fe, Co, Ni, $n = 1 - 2$, $m = 1 - 6$)

by using also the DFT. Fe_n adopt three-dimensional structures while Co_n and Ni_n clusters form planar geometries. The binding energies per atom increase with the increase of O atoms for both $n = 1 - 2$ reaching a peak at $m = n$. Datta and co-workers[23] carried out a DFT-VASP calculations of M_4O_4 and M_4S_4 clusters (M= Mn, Fe, Co, Ni, Cu). Using the pseudopotential plane wave method with the GGA approximation. For Fe_4O_4 oxide, a ring-like structure was obtained with antiferromagnetic couplings, and a total magnetic moment of 0 μ_B. The ferromagnetic state with 8 μ_B was found with an energy difference of 75 meV. The cube structure is much less stable that the ring-like one. Recently, Wang and co-workers[24] presented a first principles study of spin properties of the triplet TM_3O_3 (TM=Fe, Co, Ni) clusters and their laser-induced ultrafast spin dynamics. These results provided added information for the varieties of ultrafast optical control of magnetism in transition-metal oxide systems.

In the work reported here, we systematically studied $Fe_nO_m{}^{0/\pm}$ oxide clusters with $n = 1-$ 6 and m values until oxygen saturation is reached. We carried out DFT calculations within the generalized gradient approximation (GGA) for exchange and correlation. We focused on the structural and electronic properties, with a special emphasis on magnetism, and charge effects on the oxides. For cations, fragmentation channels were calculated and compared with previous experimental results of Molek *et al.*[13] and Li *et al.*[14] We found some nanoparticles that retain a net magnetic moment despite having a high oxidation rate. The paper is organized as follows. In section II, we describe the theoretical and computational approaches and compare some results about $Fe_2{}^{0/\pm}$ and $Fe_2O_m{}^{0/\pm}$ ($m = 1-2$) with previous ones available in literature, what allow us to benchmark our theoretical approach and to have a good starting point. In section III, we show the results that are discussed in different subsections: subsection III.1 is devoted to ground state structures and their nearest structural isomers depending on size, n, on oxidation rate, m, and on charge state. Structural properties and absolute and relative stabilities are also discussed; in subsection III.2, fragmentation channels are studied for the cationic clusters by comparing the minimum energy needed for the separation of different possible fragments; in subsection III.3 we discuss the electronic properties as well as the magnetism of $Fe_nO_m{}^{0/\pm}$. Finally, the conclusions are summarized in section IV.

II. THEORETICAL APPROACH AND COMPUTATIONAL DETAILS

We performed fully self-consistent DFT calculations using the SIESTA code[25]. For the exchange and correlation (xc) potential we used the Perdew-Burke-Ernzerhof form of the generalized gradient approximation (GGA).[26] We employed norm-conserving scalar relativistic pseudopotentials[27] in their fully nonlocal form[28], generated from the atomic valence configuration $3d^7 4s^1$ for Fe (with core radii 2.00 a.u. for s, p and d orbitals), and $2s^2 2p^4$ for O (with core radii 1.14 a.u. for s, p and d orbitals). Non-linear partial core corrections[29], which are known to be important for transition metal pseudopotentials, are included for Fe at the core radius 0.7 Å. Valence states were described using double-ζ basis sets for O and Fe with maximum cutoff radii radius 4.931 Å ($2p$) and 8.100 Å ($3d, 4s$), respectively. A $4p$ polarization orbital was also considered for Fe, with cutoff radius 8.100 Å.

The energy cutoff used to define the real-space grid for numerical calculations involving the electron density was 250 Ry. The Fermi distribution function that enters in the calculation of the density matrix was smoothed with an electronic temperature of 15 meV. We used an energy criteria of 10^{-4} eV for converging the electronic part.

In the calculations, the individual clusters were placed in a cubic supercell of $20 \times 20 \times 20$ Å^3, a size large enough to neglect the interaction between the cluster and its replicas in neighboring cells. It was considered only the Γ point ($k = 0$) when integrating over the Brillouin zone, as usual for finite systems. The equilibrium geometries resulted from an unconstrained conjugate-gradient structural relaxation using the DFT forces. Initial geometries were built by considering different arrangements of the Fe and O atoms without privileging those formed from given Fe subclusters. Thus, an exhaustive sampling of possible geometries was tested, including those in which the possibly strong Fe-O bonding prevents the nucleation of compact Fe subclusters. In addition, we tested other geometries that were built using local Fukui functions to locate O atoms in the more nucleophylic sites of the host. Fukui functions allow to determine the most reactive sites according to purely electronic arguments. The Fukui functions[30–32] f^+ and f^- are defined as

$$f^{\pm}(\vec{r}) = \left(\frac{\partial \rho(\vec{r})}{\partial N_e}\right)^{\pm}_v$$

where $\rho(\vec{r})$ is the spatial charge density, N_e the number of electrons, and the subscript indicates that the right/left derivatives have to be calculated at constant external potential, i.e. by keeping the atomic coordinates fixed. The scalar fields $f^{\pm}$ measure the local variations

in electronic charge induced by the addition or removal of electrons, and so they can be used as useful local indices of electronic reactivity. f^+ refers to the electron density response upon addition of electrons, and so it is an indicator of locally electrophilic regions which are more susceptible to nucleophilic attack; similarly, f^- locates the most nucleophilic regions within the system, susceptible to an electrophilic attack. Larger positive values of $f^{\pm}$ correspond to more reactive sites. Coupling the Fukui function with the Bader analysis, we can define atom-resolved condensed Fukui functions, $f_i^{\pm}$ for each atom i , by calculating the variation in electronic charge inside each of the Bader atomic basins. Following the standard practice, we have approximated the derivatives by simple finite differences:

$$f_{N_e}^+(\vec{r}) = \rho_{N_e+1}(\vec{r}) - \rho_{N_e}(\vec{r})$$
$$f_{N_e}^-(\vec{r}) = \rho_{N_e}(\vec{r}) - \rho_{N_e-1}(\vec{r})$$

The global minimum and low-energy isomers found for the neutral oxides are used as inputs for their charged counterparts. The ground state geometry of charged clusters not always is the obtained global minimum structure of the neutral ones, as it will be seen in the next section. Charged systems can be dealt with through the addition of a Madelung correction. Although the finite difference expressions provide the exact value for the derivative according to DFT[32], in practical calculations the expressions are not exact due to the self-interaction error of approximate exchange-correlation functionals. Nevertheless, the standard usage of those finite difference approximations is justified by the fact that approximate xc-functionals are much more accurate for integer numbers than for fractional numbers of electrons.

Structures were relaxed without any symmetry constraint until interatomic forces were smaller than 0.003 eV/$\mathring{A}$. All possible spin multiplicities and different initial ferromagnetic or antiferromagnetic arrangements for each of different structural geometry with different oxygen environment have been considered in order to be sure of the putative global minimum. In the search of spin isomers, the criterium for maximum interatomic forces was further reduced to 0.001 eV/$\mathring{A}$.

In order to understand the magnetic couplings of the iron oxides it is necessary to consider first the magnetic coupling of $Fe_2^{0/\pm}$, $FeO^{0/\pm}$ dimers, and even of $FeO_m^{0/\pm}$, since they are the basic units of the $Fe_nO_m^{0/\pm}$ clusters, as it will be seen below, and compare our theoretical approach with other DFT results available in the literature (see Table I and Table II). The preferred Fe-Fe magnetic coupling is parallel in itself. The local magnetic moments of each

TABLE I. Total magnetic moments (in μ_B) of the ground states of Fe_2 and FeO_m ($m = 1 - 2$) obtained in this work. Agreement with previous results is shown.

	Cation		Neutral		Anion	
	μ	d	μ	d	μ	d
Fe_2	7^{19}	2.18	6	2.04	7^{19}	2.11
FeO	$5^{18,19}$	1.71	$4^{15,18,20,22}$	1.67	$3^{18,20}$	1.69
FeO_2	1^{19}	1.65	$2^{20,22}$	1.62	3^{20}	1.71

iron atoms are 3 μ_B, resulting a total magnetic moment of 6 μ_B in the dimer, and an interatomic distance of 2.04 Å. For Fe_2^+ and Fe_2^- dimers, the magnetic moment is 7 μ_B and the interatomic distances are 2.18 Å and 2.11 Å, respectively, in agreement with Reilly *et al.*[19]. In general, when antiparallel magnetic couplings appear in Fe systems, it means that Fe atoms have somehow lost their identity (either they separate from each other, or they lose electronic charge and approaches electronically Mn). Moreover, the preferred magnetic Fe-O coupling is also parallel. The calculated transferred electronic charge from iron to oxygen is 0.46 e and the local magnetic moments of iron and oxygen result, respectively, 3.4 and 0.6 μ_B, giving a total moment of 4 μ_B and an interatomic distance of 1.67 Å. Wang *et al.*[22] also found a quintet state of FeO oxide with a bond length of 1.61 Å. Our results also agree with available data from other authors regarding interatomic distances and total magnetic moments[15,20]. For FeO^+ (FeO^-) a total magnetic moment of 5 μ_B (3 μ_B) is found in agreement with previous results[19,20].

FeO$_2$ results a triplet isosceles triangle as in previous results[20,22], with a magnetic moment of 2 μ_B in good agreement with earlier infrared absorption measurements combined with theory[33]. For the FeO_2^+ cation, the total moment is probably more ambiguous. The theoretical research of Schroder *et al.*[12] predicted a ferromagnetic trimer with a total moment of 5 μ_B, and FeO distances of 1.63 Å, and a spin isomer with 3 μ_B, at only 0.04 eV in energy. The doublet isomer was found at 3 eV higher in energy. However, Relly et al.[19] found a doublet ground state. Our antiferromagnetic result for FeO_2^+ is in agrement with Reilly *et al.*[19]. Notice that Schroder *et al.*[12] found that FeO_2^+ with an oxygen molecule bonded was at 0.22 eV in energy, explaining the low energy process of loss of molecular O_2 from FeO_2. For FeO_2^- our results agree with the previous ones[20], resulting a magnetic moment of 3 μ_B. Moreover, our results about dissociation energies of $FeO_m^{0/+}$ ($m = 1 - 2$) and O_2, shown in

9

TABLE II. Dissociation energies of O_2, and $FeO_m^{0/+}$ ($m = 1 - 2$). Comparison with previous experimental results is included.

Reaction	Experimental	Castelman[19]	This work
$O_2 \rightarrow O + O$	5.115[34]	6.20	5.08
$FeO \rightarrow Fe + O$	4.7 ± 0.2[35]	5.51	5.49
$FeO_2 \rightarrow Fe + O_2$	3.60 ± 0.20[36]	4.36	4.44
$FeO_2 \rightarrow Fe + O + O$	8.64 ± 0.22[37]	10.56	9.52
$FeO^+ \rightarrow Fe^+ + O$	3.53 ± 0.06[38]	4.57	4.54
$FeO_2^+ \rightarrow Fe^+ + O_2$	2.0 ± 0.5[39]	1.98	1.75

Table II, are also in good agreement with previous results. Previous results available in the literature show the antiferromagnetic arrangement of $FeO_m^{0/\pm}$ ($m = 3, 4$) upon addition of more oxygen. The neutral FeO_3 cluster is antiferromagnetic with 0 μ_B and, consecuently, the total magnetic moment decreases by 2 μ_B upon addition of each O atom for neutral FeO_m ($m = 1 - 3$) clusters[20]. This happens because the Fe atom transfers two electrons to O. FeO_m^+ ($m = 3 - 4$) are both antiferromagnetic with 1 μ_B[19]. FeO_m^- anions keep a magnetic moment of 3 μ_B up to $m = 3$, and the value does not change to 1 μ_B until the Fe atom is coordinated with four oxygens[20].

Therefore, for $Fe_2^{0/\pm}$, the ferromagnetic character is maintained regardless of the charge state. However, when the magnetic iron atom is oxided, the results about the magnetic character change and depend on the charge. For $FeO^{0/\pm}$ the magnetic moment decreases by 1 μ_B from the cationic to the anionic dimer. When the oxidation increases, for $FeO_2^{0/\pm}$, the magnetic moment increases by 1 μ_B from the cation to the anion. Moreover, although FeO_3 does not present magnetism, FeO_3^- still preserves a magnetic moment of 3 μ_B as FeO_2^- and FeO^-. Consequently, for low oxidation rates of Fe atom, the magnetic results depend strongly on the charge. Extrapolating our and previous results about $Fe_2^{0/\pm}$ and $FeO_m^{0/\pm}$ ($m = 1 - 4$) to bigger iron oxide clusters as those investigated in the present work, some trends are expected as the oxidation rate increases. Firstly, a decrease of the total magnetic moment upon oxygen addition; secondly, a significant effect of charge on the magnetism is expected. Once a good agreemet is obtained with previous studies of the basic units of the iron oxides, we are confident in the results that we present and discuss in the next section for $Fe_nO_m^{0/\pm}$ with $n = 2 - 6$.

III. RESULTS AND DISCUSSION

In this section, firstly, we discuss the main structural features and stability of the optimized iron oxides $Fe_nO_m^{0/\pm}$ (n =2-6) with different oxidation rates; secondly, we present the fragmentation paths that we will compare with experimental results. These structural features and fragmentation paths are connected with the electronic and magnetic properties that will be discussed in the third subsection.

The relative strength of the iron-iron and iron oxygen bonds is an important factor related to the stability and structure of the iron oxide nanoparticles. An electronic charge transfer occurs from the iron to the oxygen atoms, which weakens the iron-iron bonding. Moreover, with respect to iron clusters that have larger spin-polarization per atom than iron bulk, a decrease of the tendency to parallel magnetic couplings is expected for the iron oxide clusters. Due to these interrelated factors and to the non-scability of the magnetic properties with size in nanoparticles, it is necessary to perform calculations for each size and composition to obtain reliable structural, electronic and magnetic properties as well as to understand the experimental fragmentation paths.

A. Geometrical configurations and electronic properties

In the following, iron oxide clusters $Fe_nO_m^{0/\pm}$ with $n = 2-6$, will be denoted by $(n,m)^{0/\pm}$. Global minimum structures and several low-lying energy configurations are depicted in Figures $1-5$ with $n.m$-Label signature, being Label a roman number to distinguish the different geometrical isomers with n iron and m oxygen atoms. The signature $n.m$-I always corresponds to the global minimum of the neutral oxide. The ground state structure of the cationic and anionic oxides, when it is not the same, corresponds to one of the two lowest-energy isomers of the neutral. Below the structures of each (n,m) composition, the ground state geometry for the cation, neutral and anion oxides is indicated, respectively, by its corresponding label. Numbers in parentheses correspond to the magnetic moment per atom for each state of charge, which will be related with structural arrangements. Energy differences between the different geometric isomers are shown in Tables I-V of the Supplementary Information (SI). Figure 6 shows the interatomic distance of the different bonds (Fe-Fe and Fe-O) as a function of the oxidation rate, m, for each n value, for the ground state of both

neutral and charged oxides, using different colours.

There are some magnitudes related to the structural features and stability. Thus, the binding energy per atom for neutral iron oxides $Fe_nO_m^0$ is defined as

$$E_b(n,m) = [n \times E(Fe) + m \times E(O) - E(n,m)^0]/(n+m) \tag{1}$$

and for charged iron oxides $Fe_nO_m^\pm$ is defined as

$$E_b(n,m)^\pm = [E(Fe)^\pm + (n-1) \times E(Fe) + m \times E(O) - E(n,m)^\pm]/(n+m) \tag{2}$$

where $E(n,m)$ is the total energy of the (n,m) cluster. Figure 7 shows $E_b(n,m)^{0/\pm}$ for neutral and charged iron oxides, for each n value, as a function of the oxidation rate m .

The second total energy difference in neutral and charged iron oxides $Fe_nO_m^{0/\pm}$ is defined as

$$\Delta_2(n,m) = E(n,m-1)^{0/\pm} + E(n,m+1)^{0/\pm} - 2 \times E(n,m)^{0/\pm} \tag{3}$$

that is shown in Figure 8 for neutral and charged iron oxides. For a given n, the values $\Delta_2(n,m)$ as a function of m show positive peaks at m values where the (n,m) composition is more stable than their neighboring $(n,m-1)$ and $(n,m+1)$ ones against the addition or subtraction of one oxygen atom. Thus, $\Delta_2(n,m)$ is an indicator of local stability, as it is basically the curvature of the binding energy curve, which is an indictor of the absolute stability.

Before going into the structural details for each n series, we summarize general trends that are common to most of the iron oxide clusters investigated here.

a) In the initial stages of oxidation, a compact Fe_n subcluster is formed, and the preferred positions of the oxygen atoms are the bridge or hollow sites. The preference of iron-oxygen bonds can be understood from the larger iron-oxygen binding energies (5.49 eV) than iron-iron ones (3.12 eV). The absolute maximum of the Fe-O distance takes places at a m value close to the n one. Meanwhile, the Fe-Fe distance increases.

b) For $n = 2, 3, 4$ and $m = n$, ring-like structures are obtained. This trend was already discussed in our previous work for Ni oxide clusters[40].

c) In most cases for which all bridge positions are occupied by oxygen atoms, the Fe-O distance reaches relative minima. Moreover, the iron subcluster is more open but it exists,

except for some cations in which the positive charge tends to further increase the distance between Fe atoms.

d) When all bridge (hollow) sites are saturated, oxygen atoms tend to occupy top iron positions; and when there are no more top positions available, oxygen starts to be adsorbed molecularly. This happens at high values of m due to the strong Fe-O bonds.

e) Because of the charge transfer from iron to oxygen atoms, an uniform distribution of the oxygen atoms is observed. The growth mechanism tend to maximize the number of oxygen-iron bonds.

f) When all bridge and top sites are occupied by oxygen atoms, the Fe-O (Fe-Fe) distances present the absolute minimum (maximum) value. This occurs at (3,6), an iron broken triangle with six oxygen atoms at three bridge and three top positions, at (4,10), an iron tetrahedral-like broken structure with ten oxygen atoms at six bridge and four top positions, at (5,13), an iron configuration broken square pyramid-like with thirteen oxygen atoms at eight bridge and five top positions, and at (6,15), an iron triangular prism-like broken structure with fifteen oxygen atoms at nine bridge and six top positions. For these oxide clusters, Fe-O bonds are more important as manifested in the decrease of the Fe-O distance. Moreover, Fe-Fe distances show maxima values due to weak Fe-Fe bonds and, consequently, a compact iron subcluster is not identified in the oxide structures.

g) For high oxidation states in which molecular oxygen adsorption occurs, the Fe-O distance increases and Fe-Fe distance keeps large.

h) The binding energy increases upon addition of oxygen atoms, until all bridge positions are occupied by oxygen atoms. Then a plateau develops, until a m value for which all bridge and top positions are occupied, and for which the binding energy still takes a high value, with small (large) Fe-O (Fe-Fe) distances. It can be said that the covalent bonding between Fe atoms contributes less than the partially ionic Fe-O bonding to the stability of these (n, m) iron oxides. Binding energy decreases faster when oxygen starts to bind molecularly, a trend related to the large Fe-Fe and Fe-O distances.

i) The charge has an important influence on the binding energy. In the initial oxidation states, anionic oxides have higher energy values, while neutral oxides have lower values. However, from the m value for which all bridge positions have been occupied, the binding energy of cations becomes lower than that of the neutral ones. It is remarkable the high binding energy for anions, is quite higher than that for neutral and cationic oxides. This

will have important consequences.

j) Binding energies present relative maxima values when all bridge positions are occupied by oxygen atoms and also when all bridge and top positions are occupied.

k) The positive peaks in the second energy difference match the position of maximum binding energy values. Consequently, maxima are reached when oxygen atoms occupy all bridge positions, (3,3), (4,4), (4,6), (5,8), (5,9), (6,9), or most of them, (5,4) (6,4) (6,6), and when all bridge and top positions are occupied, (3,6), (3,7) (4,10), (5,13), (6,15).

l) The magnetic character (and in particular the magnetic couplings) is strongly connected to the geometrical structure and the oxygen environment. Consequently, and related with the above trends, we have identified highly stable Fe oxide clusters with a high oxidation rate that have a large total magnetic moment due to high spin polarization and parallel couplings, something unexpected in transition metal oxide nanoparticles.

Once the main general trends have been established, let us describe in more detail the structural and electronic properties for each n series. As previously states, the non-scalability at the nanoscale makes it appealing to explore each size and composition in detail and to analyze exceptions to the general trends.

1. *Iron oxides $Fe_2O_m^{0/\pm}$, m = 1-6*

Despite iron oxide dimers have been studied previously,[12,19,20,22] a systematic theoretical study on the structural, electronic properties and magnetism is appealing. Fe_2O_m, in particular Fe_2O, can be the seed of bigger iron oxides. Moreover, we extend the study of those very small iron oxides taking also into account the charge effects.

The $(2, m)^{0/\pm}$ oxide structures, with $m = 1 - 6$, are shown in Figure 1. All them have an iron dimer. The oxygen environment is the same for all charges at each oxidation rate m, except for $Fe_2O_6^-$. There is a clear tendency to maximize the number of iron-oxygen bonds. For $m = 1$, a triangle with two iron atoms and one bonded oxygen atom on bridge position is found as the ground state geometry, 2.1-I. The second oxygen bonds also on bridge position and a rhombus is found in agreement with earlier calculations.[19,20,22] The 2.2-I structure is a reference building block in the $n = 2$ series, and for $m = 2 - 5$, the charge does not influence the oxygen environment around the iron dimer. Consequently, for $m = 3$, the 2.3-I structure have the previous 2.2.I geometry, with the third oxygen atom at the top of an iron

atom. For $m = 4$, the 2.4-I structure is obtained by adding two oxygen atoms on the 2.2-I geometry, each of them at a top position of each iron atom. For $m = 5$, the lowest energy structure, 2.5-I, is found by capping an oxygen atom at top position of the previous 2.4-I geometry. Finally, for $m = 6$, the structure consists of the 2.2-I rhombus with four terminal oxygen atoms. Notice that the two O-O axes are perpendicular to the Fe_2 axis resulting the 2.6-I structure, except for the anion with 2.6-II structure, in which the four oxygen atoms are on the same plane.

The Fe-O distance increases at low oxidation values and presents the absolute maximum when all oxygen atoms occupy bridge positions at $m = 2$ (see Figure 6). However, when the oxygen atoms bind on top positions, the Fe-O distance decreases significantly as all bridge and top positions are occupied by oxygen atoms, at $m = 4$. At this oxidation rate, FeO units and their bond become more important, and Fe-O distances are nearly constant up to $m = 6$. The charge only has influence on the Fe-O distance at $m = 1$ as it is manifested in the linear structure (2.1-II) of the cation. However, the Fe-Fe distance is very sensitive to the charge (see Figure 6). In the case of neutral and anionic oxides, the minimum distance occurs at $m = 2$, when the robust rhombus 2.2-I is found. For the neutral case, when one more oxygen is added, the Fe-Fe distance increases, being quite similar for $m = 3 - 5$. The most open neutral dimer is obtained when it is saturated with oxygen, at $m = 6$. For anionic oxides, the main differences in Fe-Fe distances with the neutral case occur at $m = 3$, as a consequence of the ferromagnetic-like character of this oxide, as will be seen in the following section. The parallel coupling between the local magnetic moments of the Fe atoms exists when the distance between them is of the order of the unoxidized iron dimer. In the case of cationic oxide clusters, the Fe-Fe distances are almost constant and large along all m range, as a consequence of the ionic repulsion between the Fe atoms due to their positive charge.
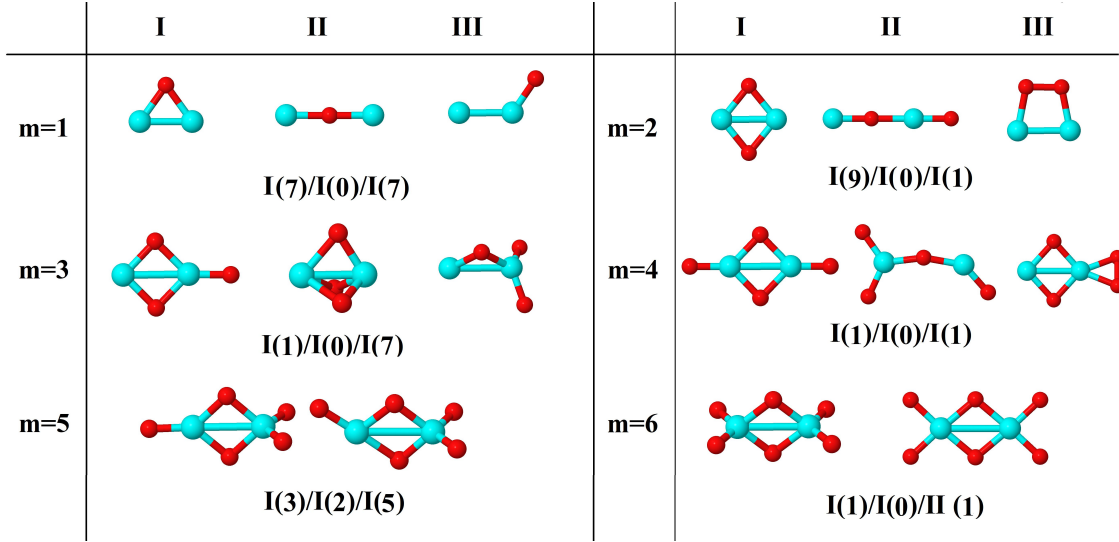
FIG. 1. (Color online) Putative ground state and first two low-energy isomers of Fe_2O_m neutral clusters with $m = 1$-6. The notation is 2.m-Label, with Label in roman letters in decreasing order of stability for each (2,m). The ground state of charged oxides, when it is not the same, corresponds to one of the two lowest-energy isomers. Below the structures of each (2,m) composition, the ground state geometry for the cation, neutral and anion oxides are indicated, respectively, by its corresponding label. Numbers in parentheses correspond to the total magnetic moment per atom for each state of charge. We note that for the cation with $m = 2$ the Fe dimer is larger than those for neutral and anion, and for anions with $m = 1, 3$ the Fe dimer is shorter (see Figure 6). Energy differences between the different geometrical isomers, for each one of the charge states, are given in Table I of the SI.

The binding energy, shown in Figure 7, increases at low oxidation rates, $m \leq 4$ ($m \leq 3$), for neutral and anionic (cationic) oxides, as a consequence of the highest strength of the iron-oxygen bonding as compared to the iron-iron one. As the oxygen content increases, the iron-iron weakens, being the FeO units more predominant, until the binding energy

16

achieves saturation. Consequently, the binding energy does not increase appreciably once each metal atom is saturated by three oxygens. Important differences with the charge are found. Anionic oxides show the highest binding energies in all m range. Moreover, they display a plateau, for high oxidation values. This behavior will be found for the rest of $Fe_nO_m^-$ series studied in this work, and will have important consequences for stability and magnetism. Moreover, although cationic oxides show higher binding energy than the neutral ones for $m = 1$, they are the least stable from $m = 3$, and this behaviour remains for all $Fe_nO_m^+$ series. Figure 8 shows the second energy difference. We see a first maximum at $m = 2$ for all charge states. Additionally, for neutral and anionic oxides a second peak is found at m=4, corresponding to the high relative stability for Fe_2O_4. Instead, the cationic oxide is less stable than their neighbours since the binding energy decreases at $m = 4$ as mentioned above.

2. *Iron oxides $Fe_3O_m^{0/\pm}$, m= 1-9*

The $(3, m)^{0/\pm}$ oxide structures, with $m = 1 - 9$, shown in Figure 2, have a triangular motif of Fe atoms, for both neutral and charged cases. Moreover, the oxygen environment is also the same for all charge states for each oxidation rate m, resulting the structure 3.m-I, except for anions with $m = 2, 4$ and for cations with $m = 8, 9$ where the 3.m-II structures are obtained.
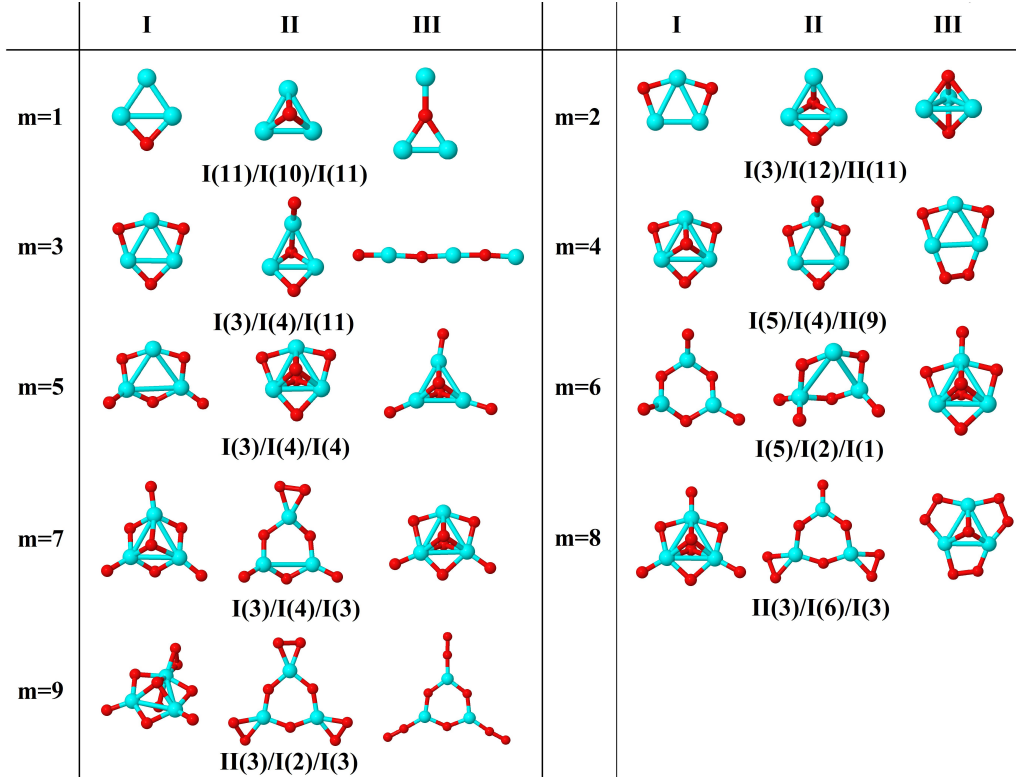
FIG. 2. (Color online) Putative ground state and first two low-energy isomers of Fe_3O_m neutral clusters with $m = 1$-9. The notation is 3.m-Label, with Label in roman letters in decreasing order of stability for each (3,m). The ground state of charged oxides, when it is not the same, corresponds to one of the two lowest-energy isomers. Below the structures of each (3,m) composition, the ground state geometry for the cation, neutral and anion oxides are indicated, respectively, by its corresponding label. Numbers in parentheses correspond to the total magnetic moment per atom for each state of charge. We note that for the cation with $m = 2$ the Fe subcluster is more open than those for neutral and anion (see Figure 6). Energy differences between the different geometrical isomers, for each one of the charge states, are given in Table II of the SI.

In the initial stages of oxidation, the preferred positions of the oxygen atoms are the bridge sites (the only exception is $Fe_3O_2^-$, already mentioned). At $m = 3$, all bridge positions become saturated (3.3-I), independently of the charge[24]. The fourth oxygen atom locates on the iron face (for the cationic and neutral oxides, 3.4-I) or it binds on top position (3.4-II structure, for the anionic case; this structure is also the second isomer in the neutral case

with a, energy difference of 0.04 eV with respect to the 3.4-I ground state). At this oxidation rate, $m = 4$, the Fe-O distance presents its absolute maximum value (see Figure 6). The next two oxygen atoms bind on top positions, and the same structures (3.5-I and 3.6-I) are preserved for all neutral and charged oxides. The Fe-O distances decrease from $m = 4$ to the $m = 6$, at which oxygen atoms occupy all possible bridge and top sites (3.6-I), and the Fe-Fe distances, that had increased almost monotonously up to this $m = 6$ oxidation rate (except for the cation with $m = 2$, with an more open Fe triangular cluster), present their maximum value (Figure 6). Moreover, the Fe-O units become more relevant and a reconstruction is observed from an initial iron subcluster (3.5-I) to a structure built by FeO subunits (3.6-I). The energy difference between this reconstructed structure (3.6-I) and the 3.5-I one adding an oxygen on top, is 0.23 eV/atom, which gives an idea of why the reconstruction is observed. The seventh and eighth oxygen atoms locate on iron face for all charge states (3-7-I) and isomers with one oxygen molecule are found. The fact that the Fe subcluster is planar favors the adsorption of more atomic oxygen, keeping the Fe-Fe distances not as larger as that of $m = 6$, as it can bee seen in Figure 6. At $m = 9$, and for all states of charge, oxygen binds molecularly. In this region, $m = 7 - 9$, Fe-O distances increase.

General structural trends are consistent with the binding energy per atom plotted in Figure 7. In general, iron oxides show higher absolute stability than nickel oxides[40] that may be important for practical purposes. The binding energy per particle increases a lot at low oxidation rates ($m \leq 3$), until oxygen occupy bridge positions (3.3-I). The maximal value is reached at $m = 6$, when Fe-O units have formed, and all bridge and top positions are occupied by oxygen atoms (3.6-I), for the neutral and anionic oxides. Further increase of the number of oxygen atoms does not enhance the binding energy. It is noteworthy that the cationic oxides, which have higher binding energy than the neutral ones in the initial states of oxidation rates, exhibit the lowest binding energy from $m = 4$, as compared to the other charge states. However, anionic oxides from $m = 3$ keep the highest binding energy, that is, they can be highly oxided while remaining very stable. Consequently, the charge of oxides is an important factor. Figure 8 shows the second energy difference, with a first maximum at $m = 3$, independently of the charge, and a second maximum at $m = 6$ (anions) and $m = 7$ (neutral and cations).

3. *Iron oxides $Fe_4O_m^{0/\pm}$, $m = 1$-14*

All ground state structures with $n = 4$ and $m = 1 - 14$, given in Figure 3, have an iron tetrahedral-like subcluster, except the anion with $m = 2$, where a planar rhombic structure (4.2-III) is formed, and for $m = 4$ and all charge states, where a ring-like planar structure (4.4-I) is obtained, with an energy difference lower than 0.4 eV with respect to the tetrahedral one. The origin of this last geometrical change is likely the fact of having a structure with all possible bridge positions occupied. Moreover, most of these charged oxides have the same 4.m-I structures as their neutral counterparts, an exception being the smallest oxidation rates, $m \leq 3$ ($m = 1, 3$) for anions (cations), where the 4.1-II, 4.2-III, and 4.3-II (4.1-II, 4.3.II) structures are more stable.
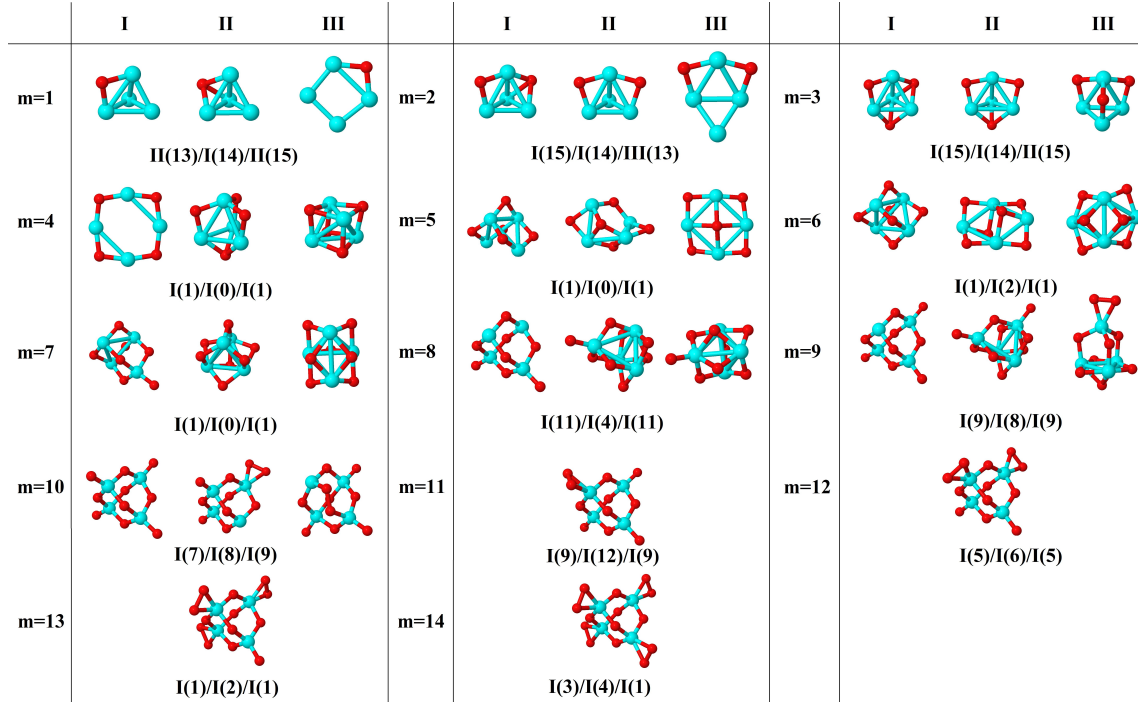
20

FIG. 3. (Color online) Putative ground state and first two low-energy isomers of Fe_4O_m neutral clusters with $m = 1\text{-}14$. The notation is 4.m-Label, with Label in roman letters in decreasing order of stability for each (4,m). The ground state of charged oxides, when it is not the same, corresponds to one of the two lowest-energy isomers. Below the structures of each (4,m) composition, the ground state geometry for the cation, neutral and anion oxides are indicated, respectively, by its corresponding label. Numbers in parenteheses correspond to the total magnetic moment per atom for each state of charge. We note that for the cation with $m = 4, 6$ the Fe subcluster is more open (nearly broken) than those of neutral and anion (see Figure 6). Energy differences between the different geometrical isomers, for each one of the charge states, are given in Table III of the SI.

The general trend of the preference of oxygen atoms for bridge (4.1-I, 4.2-II, 4.2-III) or hollow sites (4.1-II, 4.2-I, 4.3-I, 4.3-II), followed by top sites, is fulfilled. When $m = 4$, all bridge positions are saturated independently of the charge, and the Fe-O (Fe-Fe) distances reach the first minimum (maximum) value (see Figure 6), according with the formation of two Fe_2O units bound by two oxygen atoms, giving a planar ring-like atomic arrangement

21

(4.4-I). The next oxygen atoms, from five to six, bind to tetrahedral bridge positions (4.5-I, 4-6-I), and when $m = 6$ all possible bridge positions of a tetrahedral structure are occupied, the Fe-O distance reaching a maximum, whereas the Fe-Fe distance still reflects the existence of an open tetrahedral iron subcluster. The cation in an exception since it is much more open, practically broken. Then, oxygen atoms, from seven to ten, occupy the four possible top positions; in this region ($7 \leq m \leq 10$) the Fe-O distances decrease and reach the absolute minimum value at $m = 10$, with all bridge and top positions occupied. From $m = 9$, the Fe-Fe distances are noticeably large and a compact iron subcluster does not form. The main interaction is through Fe-O bonds, resulting structures that resemble that of zincblenda. No molecular absorption has been observed in the ground states until $m = 11$. From $11 \leq m \leq 14$, due to the molecular adsorption (4.m-I), Fe-O distances increase and Fe-Fe distances keep large.

Another way in which we built input structures was through the Fukui functions, as mentioned in the previous section. For example, we calculated the Fukui function for the ground state of $m = 1$, and where the Fukui function was maximum, we placed the next oxygen atom to obtain an input structure for $m = 2$, and so on . We repeated this process for all other clusters. In general, this way of building the clusters is very effective. In Figure 9, we give the Fukui function for the neutral Fe_4O_m series. We note that it is possible to build the ground state structure Fe_4O_{m+1} from the Fukui function of the previous oxide, except for Fe_4O_3 and Fe_4O_4 which depart from the rule.

The binding energy per particle increases up to $m = 6$ (see Figure 7) where all bridge positions are occupied by oxygen atoms, regardless of the state of charge, and after that it decreases. Besides, we can see a second relative maximum at $m = 10$ where all bridge and top positions are occupied (4.10-I). Just like for $n = 3$, the cationic oxides with $n = 4$ show the lowest binding energy, from $m = 6$, compared to those of the other charge states. However, anionic oxides from $m = 6$ to $n = 10$ keep a very high binding energy, much higher than that of neutral oxides and cations with any oxidation rate. When molecular adsorption takes place, the binding energy decreases, being higher for the anionic oxides. The most stable clusters against the addition or substraction of one oxygen atom are found at $m = 4, 6, 10$ for which maximum values in the second energy difference are obtained regardless of the charge state (see Figure 8). These clusters have all bridge (4.4-I and 4.6-I) and bridge and top positions (4.10-I) occupied.

4. *Iron oxides $Fe_5O_m^{0/\pm}$, m = 1-15*

For $Fe_5O_m^{0/\pm}$ and $m = 1-15$, there are mainly two families of structures shown in Figure 4: the hexahedron-like ($m = 1, 2, 6, 9, 10, 11, 15$) and the square pyramid-like ($m = 3-5$, $7-8$, $12-14$) for the neutral case, with some degree of deformation depending on the oxygen content. All the structures are three dimensional, the only exception being 5.5-II which has a ring-like planar structure and it is the ground state for the anionic oxide. Moreover, for anions, all structures are the same as for neutral oxides (5.m-I) , except the already mentioned, 5.5-II and 5.11.II. For cations, geometrical differences with respect to the neutral oxides are found at $m = 1, 6, 11$ with 5.m.II, and at $m = 2, 15$ with 5.m-III ground state structures. Structures 5.1-II and 5.2-III have oxygen atoms located on iron faces, structures 5.6-II and 5.11-II have one oxygen molecule, and structure 5.15-III has two oxygen molecules.

The general trend of oxygen atoms to occupy, firstly, from $m = 1-9$, the bridge (5.1-I, 5.2-I, 5.2-II, 5.5-I, 5.5-II, 5.6-I, 5.8-I, 5.9-I) or hollow positions (5.1-II, 5.2-III, 5.3-I, 5.4-II, 5.6-II) is fulfilled except for $m = 7$, where an oxygen atom is bonded on top position, 5.7-I.
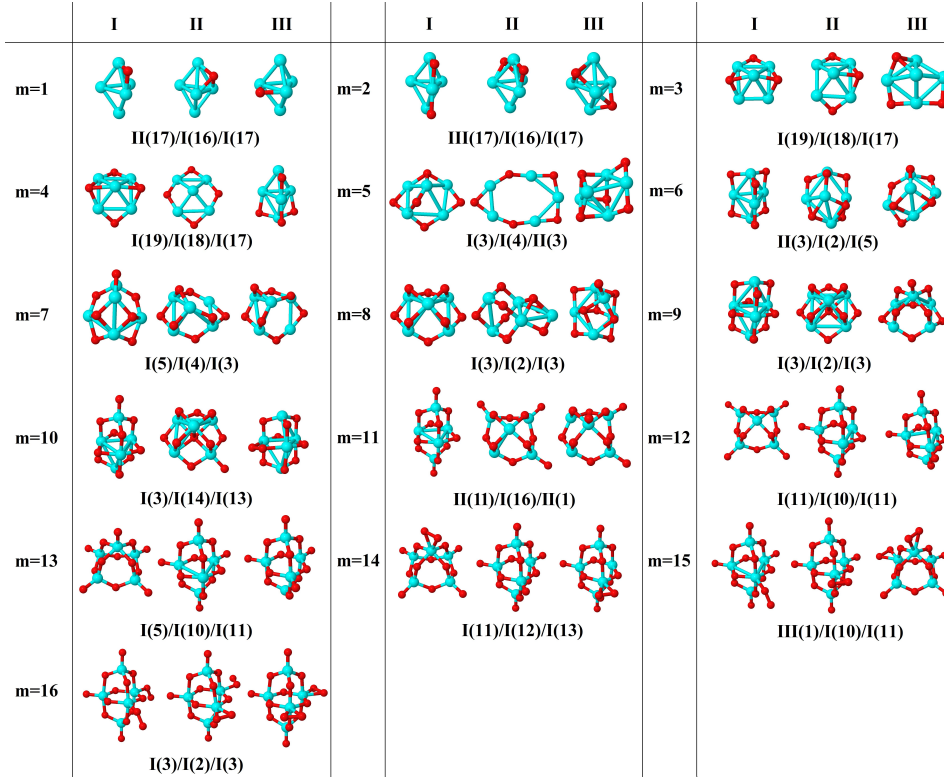
FIG. 4. (Color online) Putative ground state and first two low-energy isomers of Fe_5O_m neutral clusters with $m = 1$-15. The notation is 5.m-Label, with Label in roman letters in decreasing order of stability for each (5,m). The ground state of charged oxides, when it is not the same, corresponds to one of the two lowest-energy isomers. Below the structures of each (5,m) composition, the ground state geometry for the cation, neutral and anion oxides are indicated, respectively, by its corresponding label. Numbers in parenteheses correspond to the total magnetic moment per atom for each state of charge. We note that for the cation with $m = 6, 8, 10$ the Fe subcluster is more open, than those for neutral and anion (see Figure 6). Energy differences between the different geometrical isomers, for each one of the charge states, are given in Tables IV of the SI.

In some cases, the prevalence of the hexahedron-like or square pyramid-like structures is related to the number of bridges in each one of the geometries. The maximum number of bridge positions for the hexahedron-like structure is nine, three of them in the equatorial plane and six other bridges outside it. Oxygen atoms prefer to bind, firstly, on this other kind of bridges of the hexahedron-like structure, as it can be seen in the initial states of

oxidation, 5.1.I and 5.2.I, and for 5.6-I, with these six bridges occupied. The nine bridges are occupied at $m = 9$, resulting the 5.9-I structure. For the rest of intermediate oxidation rates, bridge (5.3-I, 5.4-I, 5.5-I 5.7-I and 5.8-I) or/and hollow (5.3-I and 5.4-I) positions of the square pyramid-like structure are occupied. The eight bridges of this other structure are occupied at $m = 8$, resulting the 5.8-I structure. In the case of this square pyramid-like structure, oxygen atoms prefer to bind first to the bridges situated on the pyramid basis, as it can been seen at 5.3-I, 5.4-I, 5.5-I and 5.7-I. Regarding the Fe-O distances, in the initial stages of oxidation, they are shorter for the bridge bonds ($m = 1, 2$) and hexahedron-like structure, increasing for the hollow cases ($m = 3, 4$) and square pyramid-like one. A more open iron subcluster is maintained until $m = 8$ and $m = 9$, where all bridge positions of square pyramid-like and of hexahedron like structures are occupied, respectively. Cationic oxides with oxygen atoms in all bridge positions are much more open at $m = 8 - 10$, similarly to cations with $n = 4$ and $m = 4, 6$. From $m = 10$ to $m = 13$, oxygen atoms bind on top positions of the hexahedron-like ($m = 10, 11$) or of the square pyramid-like ($m = 12, 13$) structures. From $m = 12$, there is not an iron subcluster, as it can be seen from the maximum of Fe-Fe distance, becoming the FeO units much more preponderant. The 5.13-I geometry has all bridge and top positions of the square pyramid-like structure occupied by oxygen atoms, what is reflected in the minimum (maximum) value of the Fe-O (Fe-Fe) distances, such as it happened for previous (3,6) and (4,10) iron oxides. The first oxygen molecule is found at $m = 14$ oxidation rate, the Fe-O distances begin to increase, and Fe-Fe distances keep large.

The binding energy per particle increases up to $m = 8$ (Figure 7) where all bridge positions are occupied by oxygen atoms. Besides, we can see a second relative maximum at $m = 13$ where all bridge and top positions are occupied (5.13-I). Anionic oxides from $m = 8$ to $n = 13$ keep high binding energies, much higher than that of neutral oxides and cations with any oxidation rate. When molecular adsorption takes place, binding energies decrease, being higher for the anionic oxides which hold high oxidation. The most stable oxides are found at $m = 4, 8, 13$ where maximum values in the second energy difference are observed regardless of the state of charge (see Fig. 8). Also, the neutral case shows a maximum at $m = 6$, with a square pyramid-like structure also found at $m = 5, 7$ neighbouring stoichiometries. These most stable clusters are obtained when all bridge (5.8-I) or most of them (5.4.I, and 5.6.I) and bridge and top positions (5.13-I) are occupied.

5. *Iron oxides* $Fe_6O_m^{0/\pm}$, *m = 1-16*

Figure 5 shows the different structural families which are obtained for $n = 6$: the octahedral one ($m = 1 - 6$), and the open triangular prism ($m = 8 - 15$). For m=7, it is obtained the structure 6.7-I which consists of a tetrahedron and a dimer with seven oxygen in bridge positions. This structure is consistent with the fragmentation spectrum obtained experimentally, as will be seen in the following subsection. The charge does not influence too much the structural geometry, resulting 6.m-I ($m = 1 - 3,6,\ 8 - 16$), for the neutral and charged cases. Only a few geometrical changes depending on the charge are found for $m = 4 - 5, 7$ ($m = 4$) for the cationic (anionic) cases. The 6.4-II prism-like structure, that is an isomer (0.03 eV) for the neutral case, results a degenerated isomer of the 6.4-II octahedral geometry for the cationic oxide, and it is also the ground state for the anionic oxide. Moreover, the 6.5-II structure is the ground state for the cation with $m = 5$.
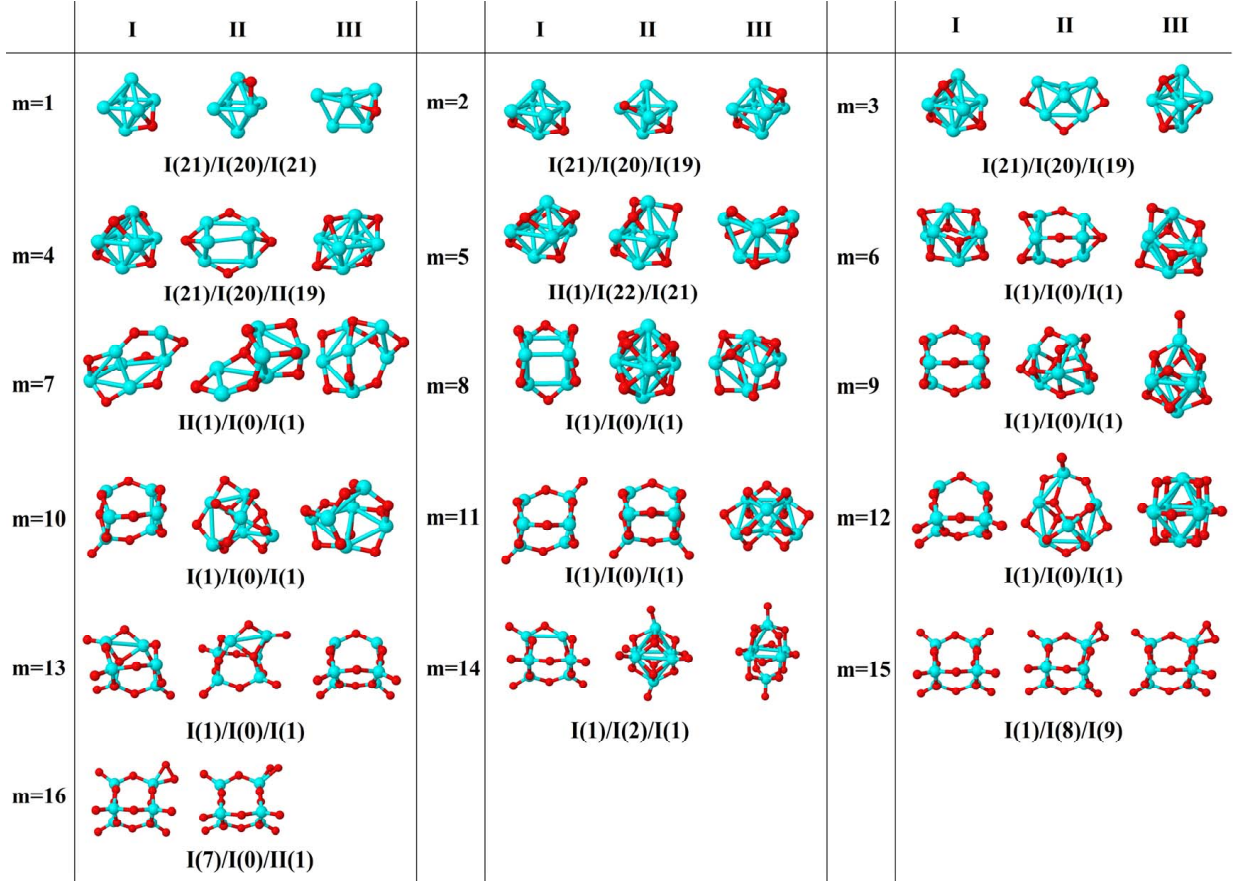
FIG. 5. (Color online) Putative ground state and first two low-energy isomers of Fe_6O_m neutral clusters with $m = 1\text{-}16$. The notation is 6.m-Label, with Label in roman letters in decreasing order of stability for each (6,m). The ground state of charged oxides, when it is not the same, corresponds to one of the two lowest-energy isomers. Below the structures of each (6,m) composition, the ground state geometry for the cation, neutral and anion oxides are indicated, respectively, by its corresponding label. Numbers in parenteheses correspond to the total magnetic moment per atom for each state of charge. Energy differences between the different geometrical isomers, for each one of the charge states, are given in Table V of SI.

Hollow positions of the oxygen are observed from $m = 1$ to $m = 6$ for the octahedral structure (6.m-I, $m = 1-6$). When the seventh oxygen atom binds, an important structural change takes place, and a tetrahedron with an additional dimer is obtained by occupying the seven oxygen atoms the bridge positions (6.7-I). From $m = 8$, a triangular prism is obtained and when the ninth oxygen atom binds, each one of the nine oxygen atoms occupies each of the nine possible bridges sites (6.9-I). Again, the structure preferred by the iron oxides

27

is the one that gets oxygen atoms occupying all bridge sites. From $m = 10$ to $m = 15$, top positions are the most favorable ones, resulting a prism triangular symmetry with all the bridge and top sites occupied by fifteen oxygen atoms, for both neutral and charged oxides (6.15-I). Molecular adsorption begins at $m = 16$, where 6.16-I structure is found for all charge states. The average Fe-O interatomic distances for the octahedral family are larger than for the triangular prism (see Figure 6). In this case, the distances decrease as the oxygen rate increases, reaching a relative minimum at $m = 15$, with all bridge and top sites occupied (6.15-I), increasing later when the first oxygen molecule is obtained (6.15.II). Additionally, the Fe-Fe average distance increases with the number of oxygen atoms up to a maximum at $m = 9$; after that, no Fe-Fe bonds are observed, prevailing the FeO units. It is worth noticing that for oxygen-rich clusters, oxygen atoms that surround the Fe atoms show local tetrahedral symmetry, reminding a diamond-like structure or the zincblenda.

The binding energy per atom increases as a function of the oxygen atoms up to $m = 9$ (see Figure 7), where all bridge sites are occupied, (6.9-I) (although we can see some relative maximum at $m = 4, 6$, with bridge bonds, especially for cations). After that, it decreases monotonously in the neutral case. As in the previous cases, the binding energy is higher for anions at any oxidation rate, particularly in the highest ones. Consequently, anionic oxides better hold the oxidation. In a consistent way, the second energy differences (Figure 8) show peaks at $m = 4, 6, 9$, being this last one the biggest, corresponding to the first structure where all the Fe-Fe bonds are broken and all bridge positions are occupied by oxygen atoms. Moreover, at $m = 15$ (the last value with the second energy difference calculated, and for which oxygen occupies all bridge and top positions) a higher value is obtained as compared with the previous one at $m = 14$.
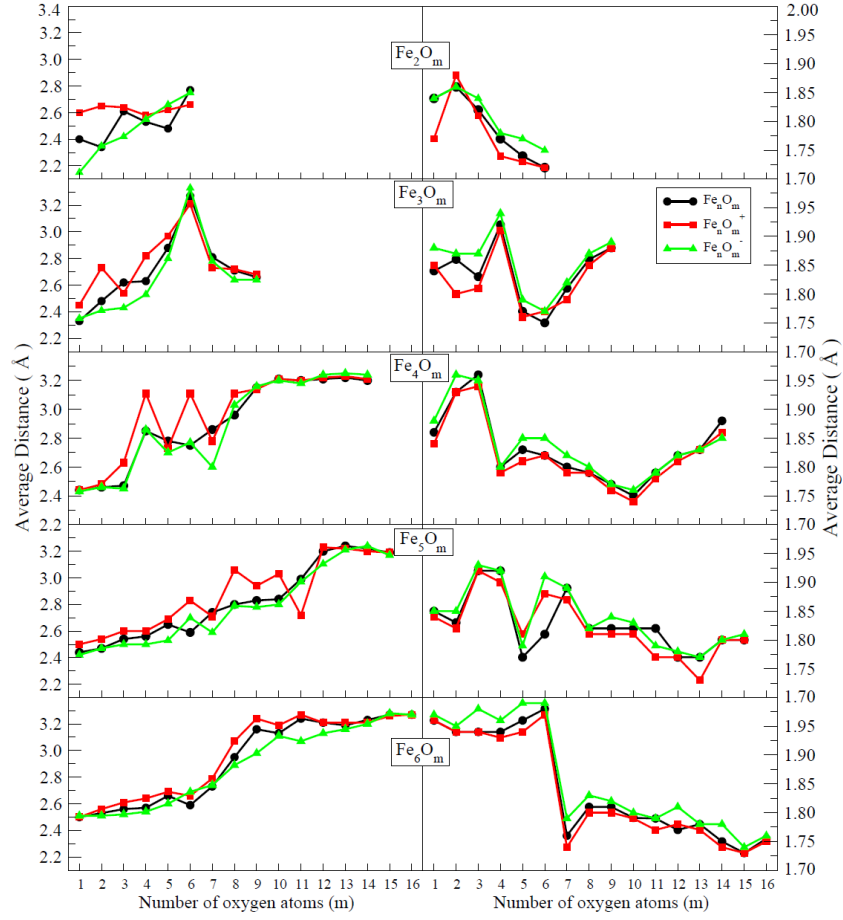
FIG. 6. (Color online) Fe-Fe (left panels) and Fe-O (right panels) average distance for $Fe_nO_m^{0/\pm}$ oxides with $n = 2 - 6$ as a function of the number of oxygen atoms, m. Red, black and green curves correspond to cationic, neutral and anionic oxides, respectively.
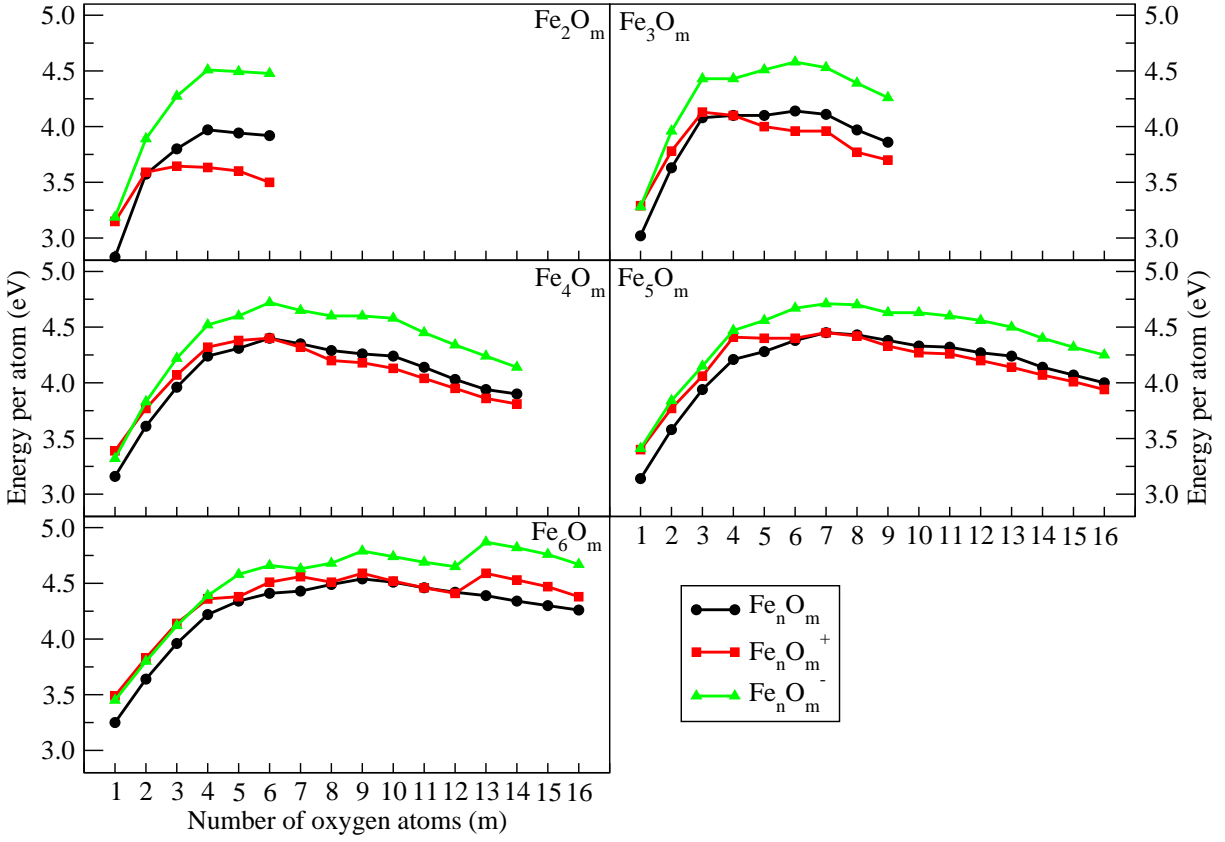
FIG. 7. (Color online) Binding energies per atom of $Fe_nO_m^{0/\pm}$ oxides ($n = 2 - 6$) as a function of number of oxygen atoms, m. Red, black and green curves correspond to cationic, neutral and anionic oxides, respectively.
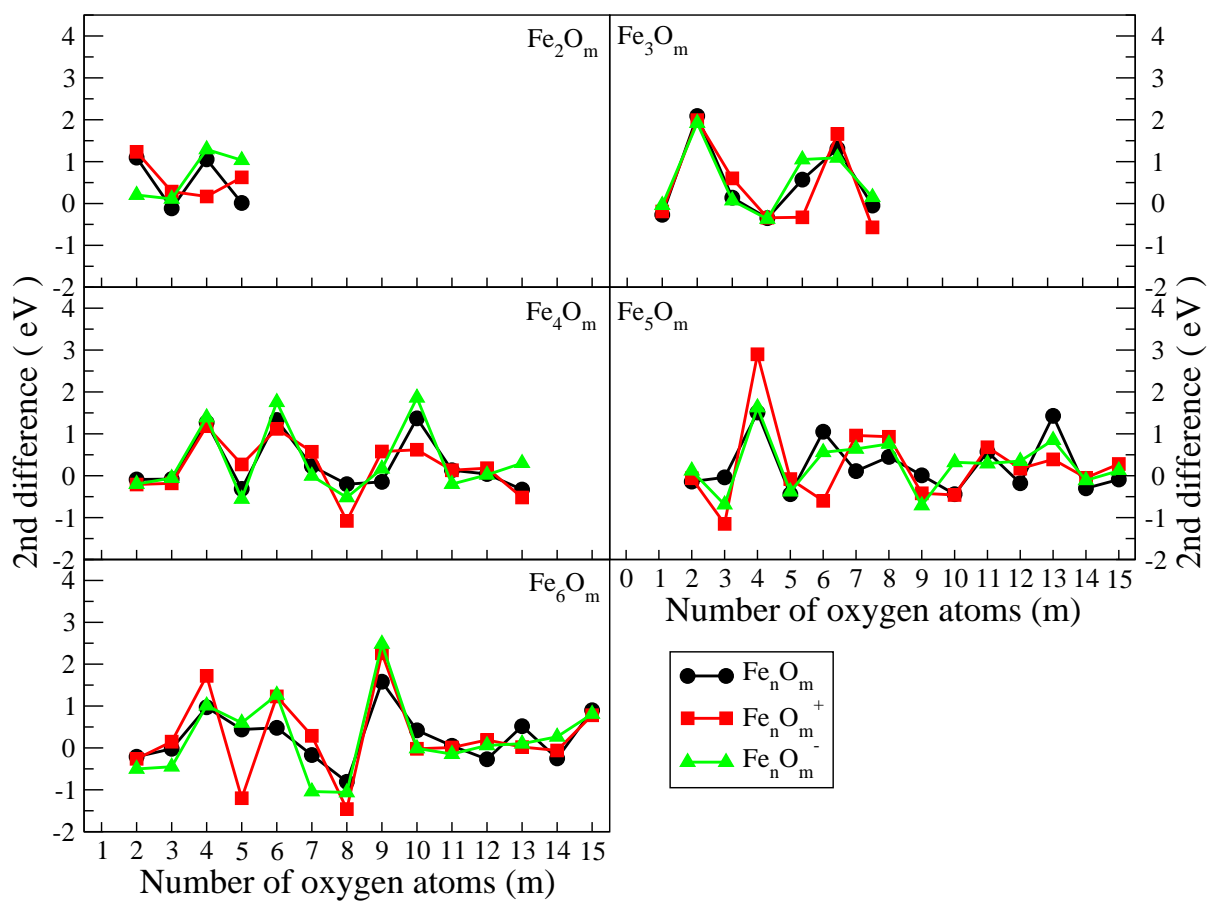
FIG. 8. (Color online) Second energy differences of $Fe_nO_m^{0/\pm}$ ($n = 2-6$) as a function of number of oxygen atoms, m. Red, black and green curves correspond to cationic, neutral and anionic oxides, respectively.
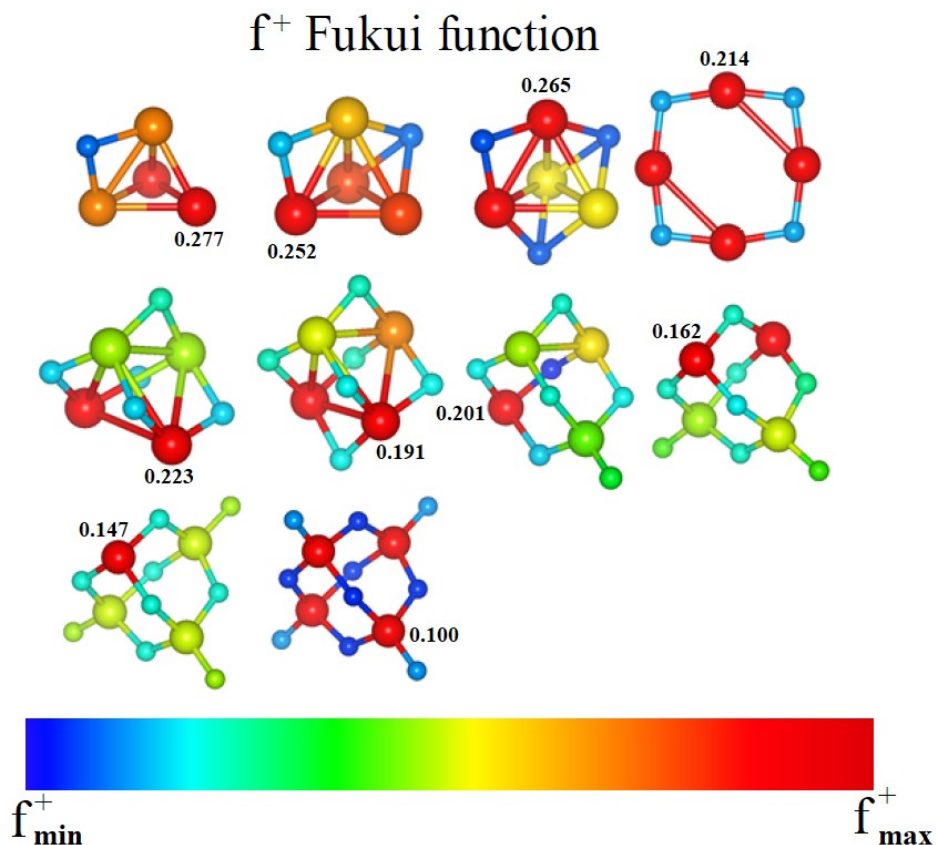
FIG. 9. (Color online) Electrophilic Fukui function f^+ for a representative sample of Fe_4O_m ($m = 1 - 10$) oxides. Small spheres represent O atoms, large spheres represent Fe atoms. Red spheres correspond to the maximum and blue spheres for minimum value of the Fukui function f^+. The maximum value of f^+ is explicitly indicated next to the corresponding atom.

B. Fragmentation channels of cationic clusters

The reactions of iron cluster cations, Fe_n^+ ($n = 2 - 18$) with O_2 was studied by Griffin *et al.*[10] and the kinetic energy dependence of these reactions over a wide range, using guided ion beam mass spectrometry, was examined. Analyzing the kinetic energy dependence of these processes, quantitative data regarding the thermodynamics of the oxidation reactions were obtained. Consequently, the oxygen bond energies, Fe_nO^+, defined as $D(Fe_n - O^+) = E(Fe_n^+) + E(O) - E(Fe_nO^+)$, were gathered. A key to this analysis was the availability of quantitative thermochemistry regarding the stability of the bare iron clusters previously measured. The energy dependence of cross sections in the threshold region was modeled[10],

where one of parameters is the threshold for the corresponding reaction, E_0. Two reactions were used to form Fe_nO^+. In the first reaction, $Fe_n^+ + O_2 \rightarrow Fe_nO^+ + O$, bond energies were derived by using the equation $D(Fe_n - O^+) = D(O_2) - E_0$. The resulting bond energies values are listed in the first column of Table III. An alternative method of deriving bond energies notes that they are related to the difference between the thresholds for reactions $Fe_n^+ + O_2 \rightarrow Fe_{n-1}^+ + Fe + O_2$ and $Fe_n^+ + O_2 \rightarrow -> Fe_{n-1}O^+ + Fe + O$. Specifically, the bond energies are calculated as $D(Fe_{n-1}^+ - O) = D(O_2) + E_0(1) - E_0(2)$. The threshold for the first reaction, $E_0(1)$, is equivalent to the bond energies of the bare iron cluster ions, $D(Fe_{n-1}^+ - Fe)$ and has been measured previously. The threshold for the second reaction, $E_0(2)$, was obtained using the analysis of cross sections in the threshold region as outlined above. The second column of Table III lists the bond dissociation energies $D(Fe_n - O^+)$ obtained from these thresholds using the two previous equations.

Moreover, the kinetic energy dependence of the reactions of Fe_n^+ ($n = 2 - 18$) with CO_2 were studied by Griffin et al.[11] in a guided ion-beam mass spectrometer. Bond energies for Fe_nO^+, $D(Fe_n - O^+)$, were measured by determining the difference between the thresholds for reactions, $Fe_n^+ + CO_2 \rightarrow Fe_{n-1}^+ + Fe + CO_2$ and $Fe_n^+ + CO_2 \rightarrow Fe_{n-1}O^+ + Fe + CO$. Specifically, the bond energies are calculated $D(Fe_{n-1}^+ - O) = D(O - CO) + E_0(3) - E_0(4)$, where $E_0(3)$ is equivalent to the bond energies of the bare iron cluster ions, $D(Fe_{n-1}^+ - Fe)$, measured previously. The threshold for the second reaction, $E_0(4)$, was obtained using the analysis of cross sections in the threshold region as outlined above. Resulting $D(Fe_n - O^+)$ bond energies are gathered in the third column of Table III. Our calculated $D(Fe_n - O^+)$ bond energies are shown in the last column and a great agreement with experimental results[10,11] is obtained.

In the context of investigating the stability of small iron oxide clusters and their dependence on the stoichiometry, Molek et al.[13] showed that photofragmentation studies of cations can be used to determine relative cluster stabilities. It is more difficult to dissociate stable clusters and, therefore, they are often obtained upon the dissociation of larger clusters. In the following, $Fe_nO_m^+$ oxides with $n = 2 - 6$ are denoted by $(n, m)^+$. In this section, we discuss the results of the fragmentation patterns of $(n, m)^+$ oxides, for which experimental results are available. To this purpose, we calculated the fragmentation energies defined as follows:

TABLE III. Bond energies of O atom in Fe_nO^+ oxides, $D(Fe_n - O^+)$. In the first two columns are included previous experimental results[10,11], where the kinetic energy dependence of some reactions was analyzed and $D(Fe_n - O^+)$ were obtained. The corresponding analized reactions are indicated in the first row.

n	$Fe_n^+ + O^2 \to$ $Fe_nO^+ + O$ *	$Fe_n^+ + O^2 \to$ $Fe_{n-1}O^+ + Fe + O$ *	$Fe_n^+ + CO_2 \to$ $Fe_{n-1}O^+ + Fe + CO$ **	This work
2	5.15 ± 0.12	—	5.1 ± 0.2	5.04
3	4.70 ± 0.13	—	4.5 ± 0.2	5.52
4	4.00 ± 0.15	—	5.9 ± 0.3	5.96
5	4.60 ± 0.15	5.10 ± 0.29	5.7 ± 0.3	5.78
6	4.00 ± 0.15	5.60 ± 0.31	5.5 ± 0.3	5.69

$$E_f(n,m) = E(n,m)^+ - E(x,y)^+ - E(n-x, m-y) \qquad (4)$$

where the first term is the energy of the cationic parent-oxide and the rest are the energies of the product-oxides, one of which resulting positively charged. A large number of possible channels were calculated, although we gathered the most favorable ones in Table IV below, and in Table VI of the SI. This process is endothermic. The channel that shows the smallest E_f will be compared with experimental results. Our definition is based on total energies of initial and final oxides and no energy barriers were considered. The biggest product-oxide carries the positive charge, except when Fe^+, Fe_2^+ and Fe_2O^+ result as product-oxides.

Our aim is to corroborate our previous DFT results about structural properties and stabilities of iron oxides by comparing them with experimental results, which only exist for the cations with $n \leq 2$[14], and with $n = 2 - 6$ and $m \geq n$[13]. Multiple photon absorption was necessary to fragment those iron oxide clusters, which is consistent with the strong metal-oxygen bond shown in the previous section. Our calculations reproduce the main features of mass spectra. The general trends can be summarized as follows: for poor-oxygen clusters $(m < n)$, the most favorable fragmentation channel is the loss of one FeO unit (Fe atom) for the smallest (largest) sizes studied, $n = 2 - 3$ $(n = 4 - 6)$. Table V reports some dissociation energies, reaching a good agreement with previous results. Oxides with $n = m$, do not eliminate oxygen, but loose a neutral FeO unit keeping $n = m$ and producing very stable species. An exception is the $(6,6)^+$ oxide whose most favorable channel is its fragmentation

TABLE IV. Calculated fragmentation energies predicted in this work. The fragmentation channels found among the most favorable ones for all $(n, m)^+$ are shown. The most favorable experimental[13] channel is indicated in bold. Fragmentation energies of low-oxided $(m < n)$ and high-oxided $(m \geq n)$ clusters are separated by horizontal lines, for each n.

	O_2	O	Fe	FeO	FeO_2	Fe^+	Fe_2^+	FeO^+	$Fe_2O_2^+$
Fe_2O^+	—	4.91	4.86	**3.91**	—	3.91	4.91	4.86	—
$Fe_2O_2^+$	4.92	5.08	7.49	**4.28**	4.50	4.50	4.92	4.28	—
$Fe_2O_3^+$	**3.70**	3.86	7.90	5.86	4.12	3.70	—	4.12	3.86
$Fe_2O_4^+$	**2.36**	3.58	9.11	5.99	5.41	—	—	—	2.36
$Fe_2O_5^+$	**1.91**	3.41	—	7.03	5.37	—-	—	—	—
$Fe_2O_6^+$	**1.62**	—	—	—	6.29	—-	—	—	—
Fe_3O^+	—	5.52	3.77	**3.36**	—	4.68	3.36	5.51	3.36
$Fe_3O_2^+$	6.16	5.71	4.57	**3.99**	4.75	4.59	4.75	5.86	4.57
$Fe_3O_3^+$	6.53	5.90	6.60	**4.97**	5.56	5.78	6.42	5.95	4.97
$Fe_3O_4^+$	4.73	**3.91**	6.90	5.02	4.56	4.87	6.98	5.15	4.56
$Fe_3O_5^+$	**1.43**	2.60	6.13	4.05	3.30	3.70	—-	2.93	2.80
$Fe_3O_6^+$	**2.02**	4.50	7.34	5.14	4.22	4.44	—-	3.66	3.95
Fe_4O^+	—	5.96	**3.82**	3.85	—	4.91	4.19	—	—
$Fe_4O_2^+$	6.53	5.65	**3.76**	3.98	5.18	4.50	4.04	6.02	5.20
$Fe_4O_3^+$	6.44	5.86	**3.72**	4.13	5.52	4.03	5.32	5.82	5.70
$Fe_4O_4^+$	6.83	6.04	5.86	**4.27**	6.85	5.83	6.54	5.53	5.94
$Fe_4O_5^+$	5.83	**4.86**	8.12	5.23	5.11	7.50	7.63	6.16	6.10
$Fe_4O_6^+$	**4.37**	4.59	8.21	7.21	5.49	7.14	8.46	7.55	5.86
Fe_5O^+	—	5.79	**3.43**	3.90	—	4.63	4.15	—	—
$Fe_5O_2^+$	6.72	6.01	**3.79**	3.95	5.58	4.80	4.10	6.10	—
$Fe_5O_3^+$	6.97	6.05	3.97	4.34	5.67	4.77	**3.81**	6.30	6.07
$Fe_5O_4^+$	8.18	7.21	**5.14**	5.69	7.22	5.81	6.79	7.44	7.22
$Fe_5O_5^+$	6.45	4.31	4.54	**3.96**	5.68	5.23	7.91	5.59	5.21
$Fe_5O_6^+$	3.63	4.39	4.40	3.49	4.03	4.40	7.35	5.08	—
$Fe_5O_7^+$	**4.31**	5.00	5.93	4.90	4.47	5.52	9.21	4.86	7.17
$Fe_5O_8^+$	**3.96**	**4.04**	7.70	4.48	4.22	5.91	10.07	5.02	6.26
Fe_6O^+	—	5.63	**4.03**	4.32	—	5.63	4.47	—	—
$Fe_6O_2^+$	6.81	6.25	**4.27**	4.79	6.25	5.62	4.88	7.34	—
$Fe_6O_3^+$	7.68	6.51	**4.74**	5.29	6.97	5.74	5.32	7.59	7.10
$Fe_6O_4^+$	7.79	6.36	**3.89**	5.60	7.33	5.66	5.51	7.55	7.62
$Fe_6O_5^+$	6.70	5.42	4.99	**3.82**	6.70	6.25	6.03	6.54	6.97
$Fe_6O_6^+$	5.40	5.06	5.66	5.05	4.55	5.85	5.88	6.77	5.86
$Fe_6O_7^+$	5.15	5.17	5.82	5.33	5.40	5.80	7.16	6.47	6.12
$Fe_6O_8^+$	3.86	4.33	5.56	4.71	4.78	5.42	7.28	5.04	4.69

TABLE V. Fragmentation energies of Fe_2O^+ and $Fe_3O_2^+$. Comparison with previous results are included.

Reaction	This work	Li[14]	Experimental
$Fe_2O^+ \rightarrow Fe^+ + FeO$	3.91	3.79	-
$Fe_2O^+ \rightarrow Fe + FeO^+$	4.86	4.44	-
$Fe_2O^+ \rightarrow Fe_2^+ + O$	4.91	4.88	5.15 ± 0.05[39]
$Fe_3O_2^+ \rightarrow FeO + Fe_2O^+$	3.99	3.68	-
$Fe_3O_2^+ \rightarrow Fe^+ + Fe_2O_2$	4.59	4.40	-

into the neutral $(3,3)$ and the cation $(3,3)^+$, both with $n = m$ and both very stable, in good agreement with experiments. The decomposition of larger oxides with $m > n$, produces a variety of product cations, but those with $n = m$ are always the most prominent and these same species are produced repeatedly from different parent ions, except the $(5,5)^+$ that appears neither in the experimental spectra of the oxygen-rich oxides with n=5, nor in the spectra of n=6. This fact is understandable, since this cluster does not present the highest stability in the n=5 series according to our calculations. For $n = 6$, and $m > n$, the fragmentation does not produce oxygen, but the structures fragment experimentally producing the subclusters that are preformed, which supports our results. Figure 10 shows the theoretical fragmentation channels predicted in our calculations, for $m \geq n$, in good agreement with experiments from Molek.[13]
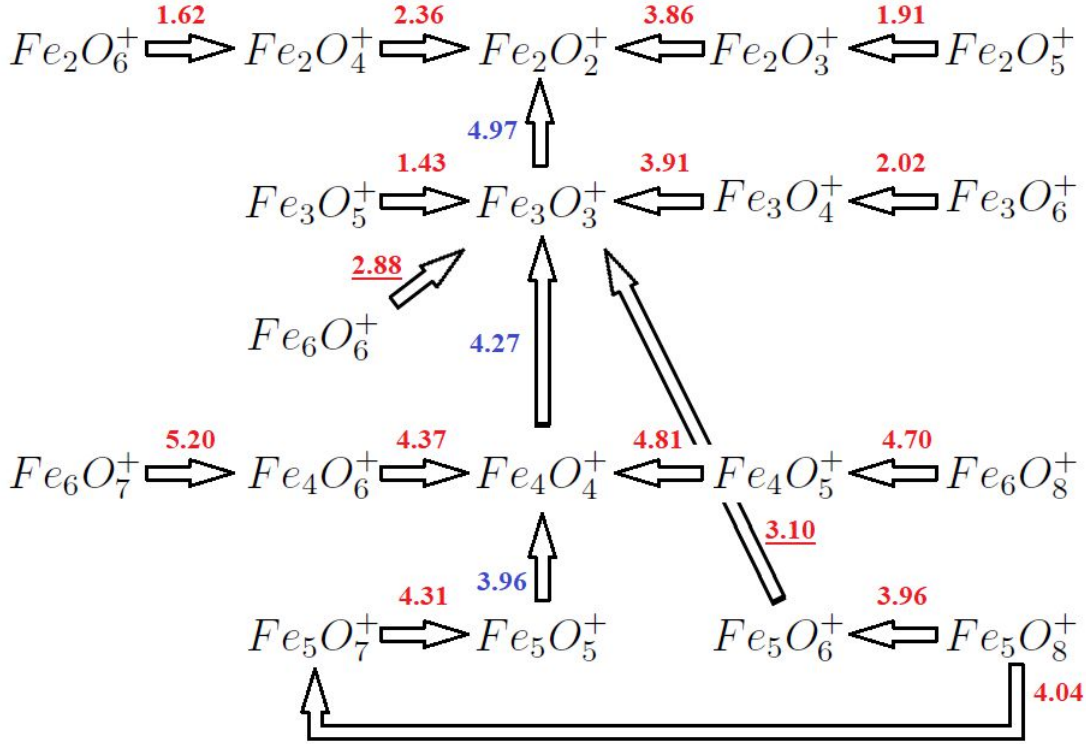
$$Fe_2O_6^+ \xrightarrow{1.62} Fe_2O_4^+ \xrightarrow{2.36} Fe_2O_2^+ \xleftarrow{3.86} Fe_2O_3^+ \xleftarrow{1.91} Fe_2O_5^+$$

$$\Big\uparrow 4.97$$

$$Fe_3O_5^+ \xrightarrow{1.43} Fe_3O_3^+ \xleftarrow{3.91} Fe_3O_4^+ \xleftarrow{2.02} Fe_3O_6^+$$

$$Fe_6O_6^+ \xrightarrow{2.88} \qquad 4.27$$

$$Fe_6O_7^+ \xrightarrow{5.20} Fe_4O_6^+ \xrightarrow{4.37} Fe_4O_4^+ \xleftarrow{4.81} Fe_4O_5^+ \xleftarrow{4.70} Fe_6O_8^+$$

$$3.10$$

$$Fe_5O_7^+ \xrightarrow{4.31} Fe_5O_5^+ \qquad 3.96 \qquad Fe_5O_6^+ \xleftarrow{3.96} Fe_5O_8^+$$

$$4.04$$

FIG. 10. (Color online) Theoretical sequential fragmentation channels predicted in our calculation. A good agreement with experimental results is obtained. Numbers in blue (red) colour indicate the fragmentation energies from $(n, m)^+$ oxides with $m = n$ $(m > n)$. The parallel fragmentation for $(5, 8)^+$, at only 0.08 eV, is also included.

1. Oxygen-poor iron oxide clusters $(n, m)^+$ $(n = 2 - 6, m < n)$

Before discussing the results for cations that we can compare with experiments more extensively ($n = 2 - 6$ and $m \geq n$), we discuss the fragmentation channels for the calculated cationic iron oxides with $m < n$. These oxides correspond to very low oxidation rates where the iron subcluster is kept, with oxygen atoms occupying bridge or hollow positions.

For $(2, 1)^+$ oxide, with a triangular structure 2.1-I, the two preferred fragmentation channels produce the $(1, 1)$ unit or Fe atom (and Fe^+ or $(1, 1)^+$, respectively) with energies 3.91 eV and 4.86 eV. These results are in good agreement with Li[14] and experimental results (Table IV). We find that for $n = 3$ and $m = 1 - 2$, the most favorable fragmentation

channel corresponds to the loss of a $(1,1)$ unit, results consistent with the 3.1-I and 3.2-I structures found (Figure 2). The loss of a neutral Fe atom is the next favorable channel at 0.41 eV and 0.58 eV, respectively. This channel, in which oxides lose an neutral Fe atom, becomes the preferred one for all $n = 4 - 6$ oxygen-poor iron oxides ($m = 1 - 3$) with $m < n$. Fragmentations are compatible with the tetrahedral, pyramidal, hexahedral and octahedral structures found (Figures 3-5). The only exception is $(5,3)^+$ whose fragmentation, by the loss of Fe_2^+ (Tabla VI, SI) instead Fe atom, produces the very stable neutral $(3,3)$ iron oxide. Moreover, from $(4,3)^+$ and $(5,4)^+$, iron fragmentations result on very stable $(3,3)^+$ and $(4,4)^+$ oxides, respectively. The second preferential channel for $n = 4 - 6$ iron oxides with $m < n$ is the loss of a $(1,1)$ unit.

2. *Oxygen-rich iron oxide clusters* $(2,m)^+$ *($m \geq n$)*

In the n=2 serie, the smallest oxide produced in experiments[13] is the $(2,2)^+$ cluster. Moreover, $(2,2)^+$ oxide was obtained from the fragmentation of $(2,m)^+$ ($m > 2$), as a consequence of its high stability in agreement with our results (Figure 8). Although the $n = 2$ mass spectra are not shown in the experimental work, the resulting fragments are indicated both in a table and in the text, although with different information. We found a rhombic structure with both oxygen on bridge positions of Fe dimer, whose bonding distance is 2.65Å. This geometry may explain why the loss of O_2 or the $(1,1)^+$ fragment is not observed in the experiments,[14] being the energy of dissociation of O_2 similar to that of the loss of the an O atom, resulting the $(2,1)^+$ fragment observed, whose bonding distance of 2.60Å is similar to that of parent oxide. The loss of O_2 requires a rearrangement to form the O_2 bond, and the loss of $(1,1)$ fragment requires the breaking of more bonds, including Fe-Fe bond, making them unfavorable from the entropic point of view, and compared to the fragmentation to the resulting $(2,1)^+$ oxide, that only require two bond breaks.

For $n = 2$ and $m > 2$, the preferred channels are the loss of an oxygen atom ($m = 3$) or molecular oxygen ($m = 4-6$), in agreement with Li[14] and Molek[13], and this fact corroborates the structures and stabilities that we have obtained (2.n-I, see Figure 1). For $m = 3$, the 2.3-I calculated structure of $(2,3)^+$ has a terminal oxygen atom added to the 2.2-II rhombic structure of $(2,2)^+$, and the calculated energy of 3.86 eV to evaporate an oxygen atom is in good agreement with Li *et al.*[14] (3.82 eV). Competing with this dissociation

pathway is the formation of $(1,1)^+$ as well as $(1,2)$, which involves the same bond breaks as the fragmentation of $(2,2)^+$ into Fe^+ and $(1,2)$, resulting a similar energy of 4.12 eV versus 4.28 eV. The calculated energy of 4.12 eV is also in agreement with Li *et al.*[14] (3.96 eV). The thermodynamically favored process is the loss of O_2, which is presumably more favorable for $(2,3)^+$ (3.70 eV) than for $(2,2)^+$ (4.92 eV), probably due to the existence of an oxygen top atom that is closer to the bridging oxygens than they are to each other in the $(2,2)^+$. However, loss of O_2 still requires a more constrained pathway and, therefore, as the modelling discussion of Li[14], it is entropically disfavored, and even more so in our case due to the required rearrangement of the rhombic structure 2.3-I to transform into the linear structure 2.1-I. For $m = 4$, the calculated ground state structure of $(2,4)^+$ starts with the rhombic structure of $(2,2)^+$ and has the two extra oxygen atoms (2.4-I); the loss of molecular oxygen is the preferred channel (2.36 eV) to fragment into very stable $(2,2)^+$. In this case, no geometrical rearrangement is necessary. For $m = 5 - 6$, the calculated ground state structures (2.5-I and 2.5-II) add additional terminal oxygens to the 2.4-I geometry. The fact that the energy required to lose O_2 from both is small, 1.91 and 1.62 eV, respectively, is consistent with the 2.5-I and 2.6-I structures found. Moreover, the $(2,2)^+$ fragment could also result from the $(2,6)^+$ cationic parent after the elimination of two oxygen molecules.

It is worth noting that small $n = 2$ iron oxides are oxygen-rich from most m values ($m > 2$), and a recurrent trend is found: the loss of oxygen, also reported by Castleman *et al.*[20] in the collision dissociation of oxygen-rich iron. This behavior supports the sequential fragmentation shown in Figure 10, resulting the cationic $Fe_2O_2^+$ iron oxide as a fragment from more oxidized species as a consequence of the high stability of this oxide (see Figure 8), which is also in keep with results from Molek[13] and Li[14].

3. *Oxygen-rich iron oxide clusters $(3,m)^+$ $(m \geq n)$*

For $n = 3$ serie, the smallest oxide produced in experiments[13] is the cationic $(3,3)^+$ fragment. At the photodissociation mass spectra (Figure 2 of Molek[13]) , the loss of O_2 is not observed. The resulting stable fragment is $(2,2)^+$. The six-membered ring with alternating Fe and O atoms (Figure 2) is consistent with the fragmentation channel that involves breaking of two FeO bonds resulting the $(2,2)^+$ fragment. The required energy is 4.97 eV, also in agreement with Li *et al.*[14] (5.22 eV). The Fe^+ peak obtained in the

experimental spectrum[13], although it may come from a sequential fragmentation from the obtained $(2,2)^+$ explained above, could also result from a parallel fragmentation of $(3,3)^+$, with an energy at only 0.81 eV higher, which would explain the high peak found for Fe^+ in the $(3,3)^+$ spectrum. Even the $(2,1)^+$ peak obtained, could also come from $(3,3)^+$ (at 0.59 eV). This agrees with Li *et al.*[14] that found three fragmentation patterns, all of which involve cleavage of two FeO bonds to yield the $(2,2)^+$, Fe^+ and $(2,1)^+$ products.

On the other hand, $(3,3)^+$ is also obtained in the fragmentation of $(3,m)^+$ (m> 3), exhibiting a high peak, at $m = 3$ in the mass spectra of $n = 3$ iron oxides with m> 3, as a consequence of the high stability of the $(3,3)^+$ oxide. Experiments[13] show that $(3,3)^+$ was even produced from larger iron oxide clusters, and that it was found as the most stable cationic iron oxide in the $n = 3$ serie. This result is in good agreement with ours (Figure 8). Likewise, the $(3,4)^+$ cluster shows a 3.4-I structure formed by adding a terminal oxygen to one of the iron atoms of $(3,3)^+$ (see Figure 2). Now, cleavage of the terminal FeO bond, losing an oxygen atom (3.91 eV), leads to the primary $(3,3)^+$ product observed[13], preserving the ring structure. In addition, $(2,2)^+$ (Fe^+) cations coming from the sequential fragmentation of the $(3,3)^+$ oxide, could also result from parallel fragmentation from the $(3,4)^+$ parent ion, with an energy difference of 0.65 (0.96) eV. Moreover, $(3,5)^+$ and $(3,6)^+$ fragment to $(3,3)^+$ (1.43 eV) and $(3,4)^+$ (2.02 eV), respectively, via the loss of molecular oxygen, in agreement with the experimental mass spectra[13]. Reilly[19,20] also reported the loss of molecular oxygen in the collisional dissociation of iron oxides rich in oxygen. These results are also coherent with our predicted structures, 3.5-I and 3.6-I (Figure 2).

The resulting sequential fragmentation of $(3,m)^+$ oxides, explained above, can explain the experimental spectra, as it is shown in Figure 10.

4. *Oxygen-rich iron oxide clusters* $(4,m)^+$ *(m $\geq$ n)*

The same type of fragmentations are also obtained for the $n = 4$ serie ($m = 4 - 6$) and our results again agree with the experiment.[13] For oxygen-rich clusters such as $(4,5)^+$ and $(4,6)^+$, the first step is the loss of one oxygen atom (4.86 eV) or molecular O_2 (4.37 eV), respectively, resulting the $(4,4)^+$ oxide, that is very stable (see Figure 8). For these two oxides (m=5-6), a sequential dissociation mechanism explain the experimental spectra[13], although, in the first case, the fragment $(3,3)^+$ could also be directly obtained from a parallel

fragmentation (5.11 eV, at 0.25 eV higher in energy) from $(4, 5)^+$, that would explain the high abundance of this oxide, indicated in bold in Table 1 of Molek *et al.*[13]. Again, the $m = n$ oxide fragments via the loss of a FeO unit, thus $(4, 4)^+$ fragments to $(3, 3)^+$ (4.27 eV). This behavior establishes that $(3, 3)^+$ and $(4, 4)^+$ iron oxide clusters are the most stable cations in the n=3, 4 series, in good agreement with experimental results[13,14] and our previous results about stabilities (Figure 8).

5. *Oxygen-rich iron oxide clusters* $(5, m)^+$ $(m \geq n)$

For the $n = 5$ serie and $m = 5, 7$, whose experimental spectra was shown (Figure 3 of Molek[13]), the same kind of fragmentation seen for n=3, 4 is found, and all seems to indicate a sequential dissociation mechanism (Figure 10). $(5, 5)^+$, with 1:1 stoichiometry, fragments via an initial loss of a FeO unit (3.96 eV) reaching the $(4, 4)^+$ oxide, that is very stable (Figure 3). This fact is consistent with the ground state structures of both systems, 5.5-I and 4.4-I (Figures 3-4). Subsequently, the steps above explained for this fragment follows and two FeO units are consecutively detached, resulting the $(4, 4)^+$, $(3, 3)^+$, $(2, 2)^+$, as reported in the experimental mass spectra. The $(5/7)^+$ oxygen-rich cluster, in the same way as previous cases for n=2-4, loss an oxygen molecule (4.31 eV) producing the $(5, 5)^+$ fragment. Following its fragmentation process, our results explain the experimental mass spectrum of $(5, 7)^+$, resulting the cationic $(5, 5)^+$, $(4, 4)^+$, $(3, 3)^+$, $(2, 2)^+$.

In the case of $(5, 8)^+$, some changes happen (Figure 10). As we will see below, for $n = 6$ (and other sizes not studied here) it is not possible to explain some experimental spectra from a single sequential process. The first step is the loss of molecular oxygen resulting the $(5, 6)^+$ fragment whose mass spectra is not shown in the experimental work. One option could be, a priori, the loss of an O atom reaching the $(5, 5)^+$ oxide (4.39 eV). However, the detachment of the neutral $(2, 3)$ fragment to give $(3, 3)^+$ only needs 3.10 eV from our calculations. Moreover $(5, 5)^+$ does not result a very stable cluster from our calculations, because it does not have all bridge or all bridge and top positions occupied by oxygen atoms. Therefore we propose that the next step for the resulting cationic $(5, 6)^+$ fragment is to reach the very stable cationic $(3, 3)^+$ oxide by losing the neutral $(2, 3)$ fragment. Then $(3, 3)^+$ oxide would follow the steps explained above. Moreover, in the $(5, 8)^+$ spectrum, there are some additional small peaks and a peak associated with $(4, 4)^+$, that is not as high

41

as the one associated with $(3, 3)^+$. We propose a parallel fragmentation from the $(5, 8)^+$ parent (Figure 10), losing an oxygen atom (with an energy of 4.04 eV, just 0.08 eV higher than that of the first fragmentation to $(5, 6)^+$) and resulting the $(5, 7)^+$ oxide that fragments to $(5, 5)^+$ and consecutively to the very stable $(4, 4)^+$ oxide, which shows[13] a higher peak than the previous less stable $(5, 7)^+$ and $(5, 5)^+$ fragments (whose signal is only slightly noticeable). Afterwards, $(4, 4)^+$ fragment follows its fragmentation process as explained above, what would also explain the larger height of the experimental peak associated to the $(3, 3)^+$ fragment. These results are consistent with the fact that the $(5, 5)^+$ oxide is not as stable (Figure 8 and experimental $(5/8)^+$ spectrum[13]), and that not all clusters with 1:1 stoichiometry are those with a very high stability as we have seen in our previous section.

6. *Oxygen-rich iron oxide clusters $(6, m)^+$ $(m \geq n)$*

One noticeable difference in the dissociation patterns for both groups is that the tendency to lose O_2 is no longer observed (Figure 4 of Molek[13]). The highest peak in the $(6, 6)^+$ mass spectrum is the corresponding to $(3, 3)^+$ fragment. We found a good agreement, and the most favorable channel is the $(6, 6)^+$ fragmentation into two very stable oxides, $(3, 3)$ and $(3, 3)^+$ with only 2.88 eV. Then, the resulting $(3, 3)^+$ oxide can fragment as explained above and the first part of the mass spectrum is reproduced. Moreover, Molek *et al.*[13] found very small peaks, resulting two channels with oxide-products, $(6, 5)^+$ and $(5, 6)^+$, that are mutually exclusive in a sequential fragmentation process, and can only occur in a parallel fragmentation process, reaching the $(3, 3)^+$ fragment. Other oxide-products that only could be explained from a parallel fragmentation process were also experimentally found[13] for $n = 7$.

The fragmentation of $(6, 7)^+$ and $(6, 8)^+$ essentially jumps over the possible $n = 5$ fragments. $(6, 7)^+$ produces instead the $(4, 6)^+$ and $(2, 1)$(5.20 eV, Table VI of SI, which is consistent from structure 6.7-II obtained with the preformed 4.6-I and 2.1-I subclusters. After, $(4, 6)^+$ fragments into $(4, 4)^+$. We found both oxides as the most stable ones for the $n = 4$ serie (Figure 8), with all bridge positions occupied by oxygen. Then, $(4, 4)^+$ follows the fragmentation process explained above reproducing the experimental mass spectrum. The $(6, 8)^+$ oxide produces the $(4, 5)^+$ one after the release of $(2, 3)$ fragment (4.70 eV). This type of fragmentation was also found for $(5, 8)^+$, and 2/3 stoichiometry is the same as that

of common bulk phase as was also indicated in the experiments[13]. Although for $(6,7)^+$ and $(6,8)^+$ we find more favorable energetic channels related to the loss of oxygen, the existence of high energy barriers, probably due to structural changes, should experimentally prevent those channels, due to the geometric arrangement of both oxides, $(6,7)^+$ and $(6,8)^+$, with the resulting experimental fragments as preformed subclusters.

In general, the fragmentation process is consistent with a sequential mechanism (Figure 10), with few exceptions such as the $(5,8)^+$ spectrum and the small peaks that are experimentally found in the $(6,6)^+$ spectrum. Moreover, although the $n = 7$ series is not studied here, experiments also found some fragmentation channels that can only be explained from a parallel fragmentation mechanism. We also found channels close to the most favorable one, which could explain the large height of some peaks. On the other hand, the above results about fragmentation energies are in keep with the trends discussed in the previous section about structural arrangements and stabilities from the calculations of binding energies and second energy differences: i) For low oxidation rates $(n < m)$ where there is a Fe subcluster with some oxygen atoms, Fe or FeO can be released. ii) The $(2,2)^+$, $(3,3)^+$, and $(4,4)^+$ oxides are very stable, with all bridge positions occupied, and are most often obtained from larger clusters. They fragment by releasing a FeO unit and moving on to the previous one. iii) The most favorable channel for the $(6,6)^+$ oxide, that do not have all bridge positions occupied, is the one leading to two neutral and charged $(3,3)$ clusters. iv) The oxygen-rich clusters with $n = 2 - 5$ and $m > n$, with an open iron subcluster, release an oxygen atom or O_2 until they find a very stable oxide, usually with $m = n$ (or $(4,6)^+$, which also has all bridge positions occupied and exhibits a high stability from our calculations).v) Oxygen-rich clusters with n=6, fragments into two pre-formed subclusters in their geometric arrangement.

C. Magnetic properties

We discuss here the magnetic properties of iron oxide clusters with particular focus on their net magnetic moment as a function of the oxidation rate. Figure 11 shows the total magnetic moment of $Fe_nO_m^{0/\pm}$ ($m = 1 - 6$) as a function of the oxygen rate m, for each n value. Moreover, in Figures 1-5, and for each (n, m) values, total magnetic moments are given in parenthesis for each charge state, to better identify possible relations with

the structural arrangements. For all n values, there are, in principle, two different initian magnetic phases depending on the oxygen concentration (see Figure 11). The first one (low oxygen concentration) is a high magnetic phase. The second one (high oxygen concentration) is a low magnetic phase. But, as we will see, a further unexpected phase with magnetic reentrance may arise at an even higher oxidation rate.

1. Small iron oxides and general trends

For $Fe_2O_m^{0/\pm}$ ($m = 1 - 6$), the magnetic character strongly depends on the charge state. Neutral oxides, with 2.m-I structures (Figure 1), are always antiferromagnetic, with a total magnetic moment equal to zero for all oxidation rates, except in the case of $m = 5$, where a value of 2 μ_B is reached. Notice that for Fe_2O a close magnetic isomer is found at only 0.02 eV with 6 μ_B and local magnetic moments of 2.92 μ_B and 0.16 μ_B for iron and oxygen atoms, respectively. Earlier works found 0 μ_B[22] and 6.8 μ_B[15] for Fe_2O, which is an important building block to be found in larger iron oxides. We emphasize that the fact that this antiferromagnetic unit has a ferromagnetic isomer so close in energy, will be reflected in the formation of larger oxides such as Fe_4O_m ($m = 4 - 6$), and, in general, those that have most of their bridge positions occupied by oxygen atoms. Cationic $n = 2$ oxides, with 2.m-I structures (Figure 1) are always antiferromagnetic with total magnetic moments equal to 1 μ_B (3 μ_B, for $m = 5$), expect for $m = 1, 2$ with high magnetic moments of 7 μ_B and 9 μ_B, respectively. These values are due to the parallel alignment of Fe spins and also with oxygen, and it was also found before[15], although for $Fe_2O_2^+$ ($Fe_2O_5^+$), we found an antiferromagnetic isomer[19] with 0 μ_B at only 0.007 eV (0.05 eV). Anionic $n = 2$ oxides have a ferromagnetic behaviour exhibiting high magnetic moments equals to 7 μ_B at the initial stages of oxidation (m=1,3), and again for $m = 5$ the magnetic moment (5 μ_B) is higher than that of the antiferromagnetic neighbours. For $m = 1$ the antiferromagnetic isomer is at only 0.07 eV. We also found antiferromagnetic isomers[20] for $m = 3, 5$ at only 0.03 eV and 0.09 eV. This small energy difference between antiferromagnetic and ferromagnetic isomers, will be preserved on bigger clusters, as we will seen below.

In relation to the behavior of larger Fe oxides, it is remarkable the strong influence of charge on the magnetic character. In this sense, there are low-energy spin excitations. On the other hand, when an oxygen atom is added on top position in the Fe dimer (2.1-III

geometry) it results in a ferromagnetic unit (see SI, Table I). This behavior, that can also be seen for the 2.3-III geometry (SI, Table I), for both neutral and charged cases, will have a significant impact on oxides with high oxidation rates that have not yet reached saturation, as we will see. Moreover, the ferromagnetic character for $n = 2$ at low oxidation rates will also be found for $n = 3$ anions, and for the rest of iron oxides sizes ($n = 4 - 6$) for all charge states. The reentrance of magnetism for $n = 2$, at $m = 5$, after the antiferromagnetic phase at $m = 4$, will also be a finding for larger clusters, where a ferromagnetic region will be found for several oxidation values after the antiferromagnetic phase.

For $n = 3$, the negative charge supports the ferromagnetic character upon addition of oxygen atoms, from $m = 1$ to $m = 4$. This effect, related to the negative charge, was already described above for FeO_m^- ($m = 1 - 3$). However, for neutral and cationic oxides, the ferromagnetic character also remains until low oxidation rates, $m = 2$ and $m = 1$, respectively. Although for $n = 3$, two phases, ferromagnetic and antiferromagnetic, can be observed, a very slight emergence of magnetic character for $Fe_3O_6^+$ and Fe_3O_8 is found.

For $n = 4 - 6$, in addition two both high and low magnetic phases, two further phases appear, resulting four magnetic phases in total (see Figure 11). For $n = 4, 5$, both neutral and charged oxides, and for $n = 6$, both neutral and anionic oxides, are ferromagnetic from $m = 1$ to $m = n - 1$. The first ferromagnetic region extends up to $m = 4$ in the case of $n = 6$ and cationic oxides, probably due to the different oxygen environment. There is a second antiferromagnetic region, for all charge states. The third one consists of a reentrance of the magnetic moment at about $m = n + 5$, since the charge also influences the magnetism for $n = 4 - 6$, especially at oxidation rates that are in the limit between different magnetic regions. In the fourth phase, an antiferromagnetic behavior is observed again.

In general, upon addition of oxygen on iron clusters, they change from genuine ferromagnetic iron clusters with some oxygen atoms around them, to clusters formed by Fe_2O units with bridging oxygen atoms and an antiferromagnetic character, towards clusters of ferromagnetic FeO units in which there are no long bonds between iron atoms, to finally reach oxygen saturation with the formation of oxygen molecules, increasing both Fe-O and Fe-Fe distances, and consequently losing stability.
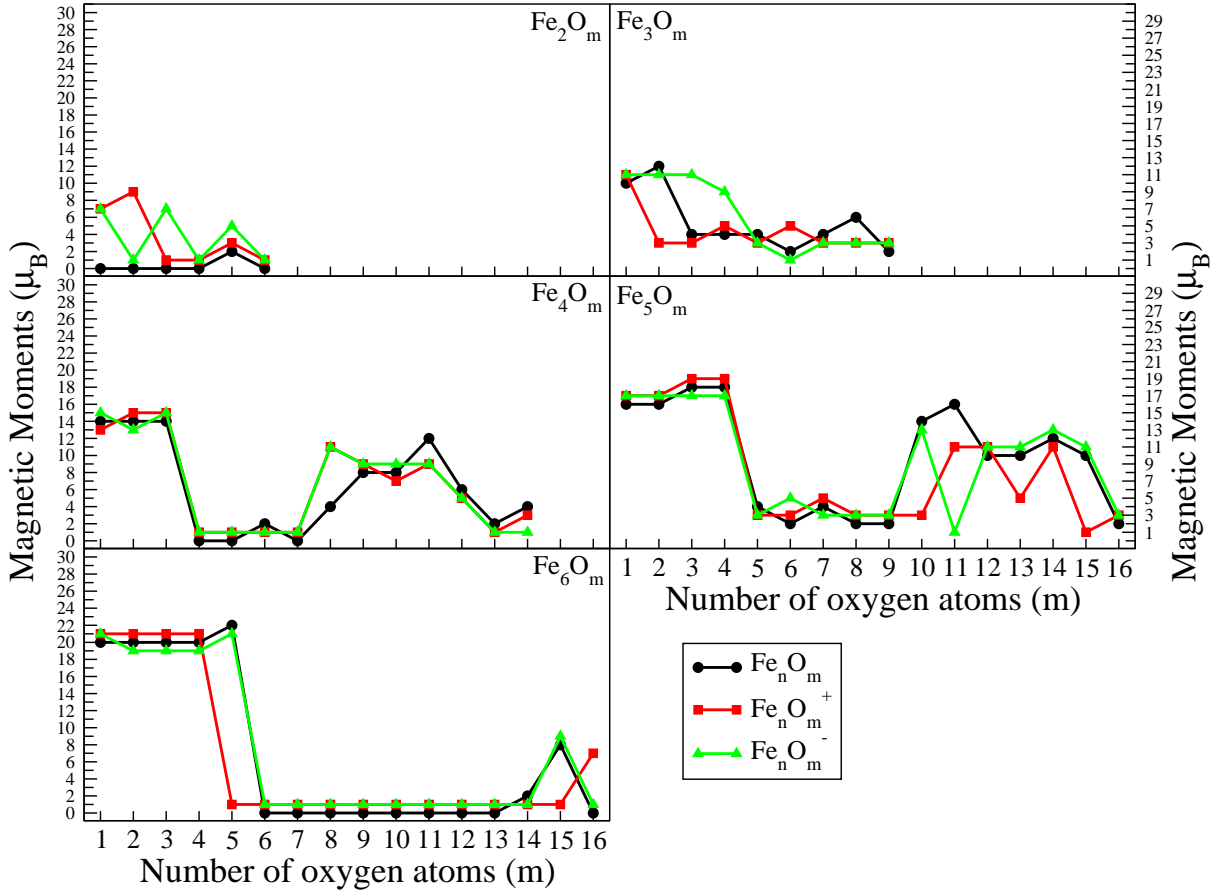
FIG. 11. (Color online) Total magnetic moment of $Fe_nO_m^{0/\pm}$ ($n = 2 - 6$, m = 1-15) as a function of the oxygen rate, m. For each n value, curves given in different colours correspond to each of the charge states: cationic (red), neutral (black) and anionic oxides (green)

.

2. *Iron oxides $Fe_4O_m^{0/\pm}$, $m = 1 - 14$*

We analyse in detail the magnetic behavior of the $Fe_4O_m^{0/\pm}$ oxide clusters to visualize and understand the different magnetic behavior depending of the oxidation rate, m. We identify four magnetic phases: (i) for $m = 1 - 3$, the total magnetic moment is high: 14 (13 or 15) for neutral (charged) oxides; (ii) for $m = 4 - 7$, the total magnetic moment is low: 0 (1) for neutral (charged) oxides, except for the neutral oxide with $m = 6$ with 2 μ_B (the spin isomer with 0 μ_B is at 0.04 ev). For $m = 8$, we found an intermediate magnetic moment ($4\mu_B$) for the neutral oxide and a high magnetic moment ($11\mu_B$) for the charged

46

oxides; (iii) for $m = 9 - 11$, the total magnetic moment is again high: 8, 12 (7, 9) for neutral (charged) oxides. For $m = 12$, we found again an intermediate magnetic moment: 6 (5) for the neutral (charged) case; (iv) for $m = 13 - 14$ we found low total magnetic moments: 2 (1 or 3) for neutral (charged) oxides. In the case of $m = 16$, although the total moment is 4 μ_B, spin isomers with 2 and 0 μ_B are found at only 0.02 and 0.06 eV, respectively. In any case, the magnetic coupling between the four iron atoms is antiparallel. Moreover, and to show either the clearly established ferromagnetic or antiferromagnetic character or the competition between both, Figure 12 shows the energy differences between the spin isomers and the ground state solution, as a function of the total magnetic moment, for neutral Fe$_4$O$_m$ oxide, with $m = 1 - 14$. Figure 12 displays, on the one hand, clear ferromagnetic states in the first phase and in the third one at $m = 10 - 11$, and, on the other hand, clear antiferromagnetic states in the second one with $m = 5 - 7$ and in the fourth region at $m = 14$. However, low-lying isomers with different magnetic behaviour are found at the beginning or ending of each of the four regions. In those limits, the charge has an important influence and the total magnetic moment can change depending on it.
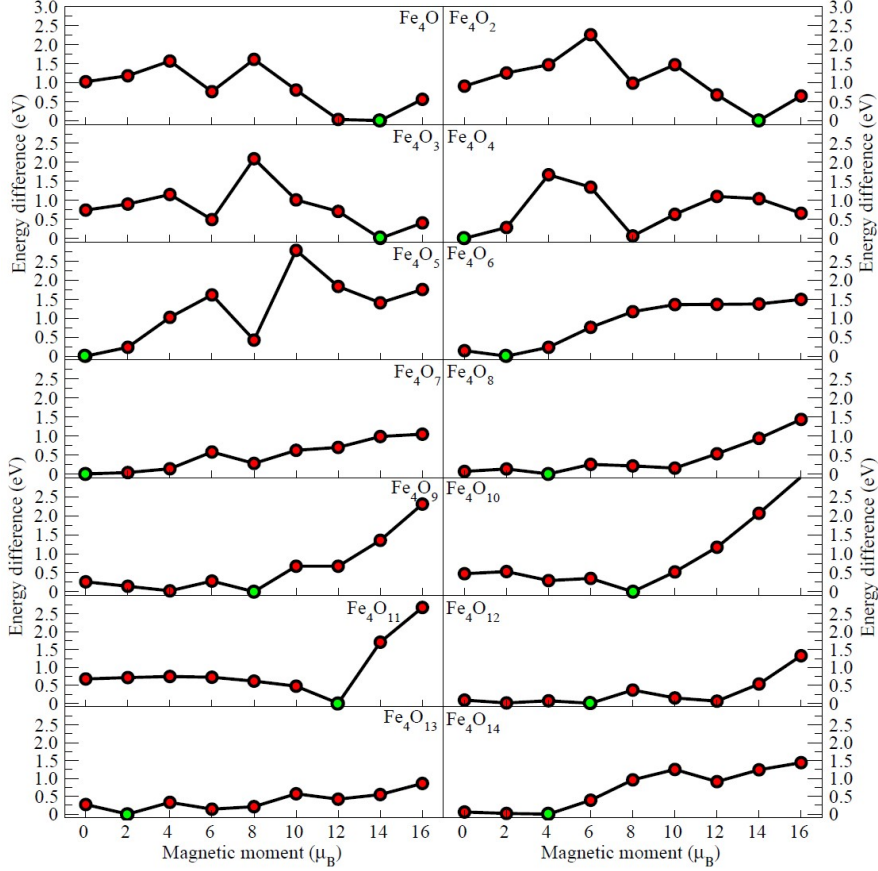
FIG. 12. (Color online) Energy difference between the spin isomers and the ground state solution (green circle, 4.m-I structure) as a function of the total magnetic moment for neutral Fe_4O_m ($m = 1 - 14$) oxides. Each pannel corresponds to a given oxygen composition, m.

The magnetic phases are closely related to the structural geometry, to the number of atomic oxygen bound at hollow-bridge and top positions (oxygen environment), and to the number of oxygen molecules formed. There is also a relationship of all these structural and magnetic properties with the stability of the oxides, as it will be seen below. Figure 13 shows, for the $n = 4$ neutral case and for each oxidation rate $m = 1 - 14$, total and local magnetic moments in each one of the Fe and O atoms of the corresponding geometrical structure. The four magnetic phases described above, $m = 1 - 3$, $m = 4 - 8$, $m = 9 - 11$, $m = 12 - 14$, are indicated with black, red, green and blue colors, respectively, and highlighted in the $n = 4$ graph of Figure 11 included also as an inset in Figure 13. In the first ferromagnetic phase, few oxygen atoms bind on bridge sites of the iron cluster. In the second antiferromagnetic phase, almost all ($m = 5$) or all ($m = 4, 6$) bridge sites of the cluster are occupied. After

48

that, there is some oxygen atoms (one for $m = 7$ and two for $m = 8$) that bind on top positions. In the third ferromagnetic phase, almost all ($m = 9$) or all ($m = 10$) top positions are already occupied by oxygen atoms and it appears the first oxygen molecule ($m = 11$). In the fourth phase, two, third and four molecules are bonded ($m = 12, 13, 14$), until the structure is completely oxygen-saturated at $m = 14$.
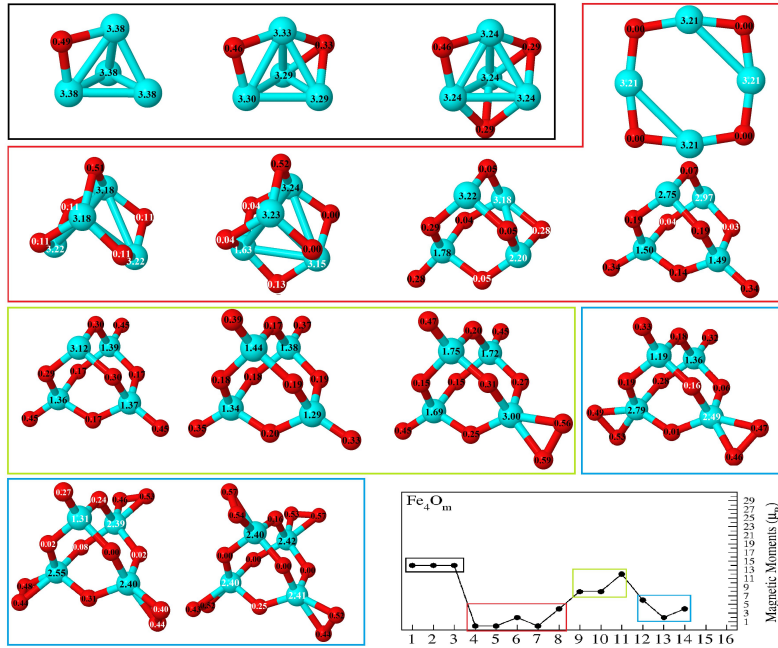

FIG. 13. (Color online) Ground states of neutral Fe_4O_m ($m = 1 - 14$) oxides. Local magnetic moments of Fe and O atoms are indicated. Numbers in black (white) indicate spin up (down) polarization. The $n = 4$ graph of Figure 11 is included as an inset.

Besides the different total magnetic moment of each of the four magnetic phases, Fe atoms present different local moments in each one of them. In the first phase, the magnetic couplings are parallel and the high total magnetic moment of the oxide clusters, 14 μ_B, is due to high spin polarization in the iron atoms. The local magnetic moments, 3.4 (Fe) and 0.5 (O), are similar to those of the FeO dimer (3.4 μ_B in Fe and 0.6μ_B in O). It can be seen from Figure 12 that the ground state has clearly a high magnetic moment. The compact iron

49

subclusters are preserved (see Figure 6) and Fe-Fe couplings are parallel, like in the bare Fe clusters. The oxygen atoms bind on some bridge or hollow positions. In the second phase, the low magnetic moment is due to high spin-polarization (about 3.2 μ_B, or 1.5-1.7 μ_B for iron atoms with top oxygen atoms) but with antiparallel couplings. Oxygen atoms that bind on bridge of iron atoms with antiferromagnetic coupling are, practically, magnetically frustrated. In this magnetic phase, most of the bridge positions ($m = 5$) or all ($m = 4, 6$) of the iron subcluster are occupied. The $m = 4$ oxide shows antiferromagnetic-like coupling between the four iron atoms, with all oxygen atoms magnetically frustrated. We highlight the $n = 5-6$ antiferromagnetic oxides, where the iron subclusters are still preserved although more open (Figure 6). Their ground states has clearly an antiferromagmetic character, as it can be seen from Figure 12. They can be seen as sub-divided into two Fe_2O ferromagnetic parts, one part with spin up and the other one with spin down, and, consequently, with an antiferromagnetic coupling between them; the oxygen atoms that are between these two sub-parts have zero , $m = 5$, or almost zero magnetic moment, $m = 6$ (an spin isomer with zero magnetic moments is at 0.04 eV, see Figure 12). Both iron oxides with all bride positions occupied by oxygen ($m = 4, 6$) present maxima in the second differences in energy, which reflects their high relative stability, and the $m = 6$ oxide has also the maximum value of binding energy. Then, for $m = 7$, an oxygen atom binds on top positions and for $m = 8$ the total magnetic moment increases (4 μ_B) and the energy difference between the low and high magnetic spin isomers becomes smaller (see Figure 12). In the third phase, a reentrance of the magnetic moment is found which is an unexpected trend in transition-metal oxides. The high magnetic moment comes from parallel couplings, but iron atoms have low local magnetic moment (low spin polarization region). Local moments of iron are lower than those of previous phases as a consequence of its high oxygen coordination (similarly as FeO$_m$ studied in the second section), and decrease from 3.1 μ_B to 1.3 μ_B, the value reached by those iron atoms with oxygen bound at top positions. Also, local magnetic moments of oxygen atoms become lower when there are oxygen atoms bound at top positions. A minimum value of FeO distance occurs at $m = 10$, and local moment of oxygen (0.3-0.4 μ_B) are closer to that in the FeO unit (0.6 μ_B). FeO units become more preponderant. In adition, a compact iron subcluster can not be identified (see Figure 6). At this third ferromagnetic phase, iron oxides are more similar to clusters of ferromagnetic FeO units bonded by oxygen atoms than to iron clusters with adsorbed oxygen atoms like in the first

ferromagnetic phase. We highlight the ferromagnetic Fe_4O_{10} oxide, with a high oxidation rate and a total magnetic moment of $8\mu_B$. Fe_4O_{10} presents a maximum in the second total energy difference and a relative maximum of the binding energy with still a high value, higher than those in the first ferromagnetic phase. This iron oxide has all possible bridge and top positions occupied. Finally, in the fourth antiferromagnetic phase, two ferromagnetic oxided subclusters can be again identified, with magnetic moments in opposite directions, and the oxygen atoms, located between those sub-clusters, are magnetically frustrated. There is not an iron subcluster. Oxygen binds molecularly, so that Fe coordinates with O_2, which weakens the Fe-O bonds (because the oxygen bond of O_2 is strong). FeO units become less preponderant and the Fe-O distance increases reaching similar values to those of the first phase. We highlight Fe_4O_{14}, with all bridge and top positions occupied and four oxygen molecules, with a clearly antiferromagmetic ground state (Figure 12). Low-lying spin isomers with 0 μ_B and 2 μ_B, at 0.06 eV and 0.02 eV, respectively, are found.

Based on the above results, we identify three particularly interesting Fe oxide clusters due to their high global and relative stability, that exhibit different magnetic characters. The planar (4,4) oxide, with Fe_2O units antiferromagnetically coupled by magnetically frustrated oxygens (indirect exchange), and (4,6) a tetrahedral iron motif also formed by two Fe_2O units antiferromagnetically coupled by four oxygens, practically, magnetically frustrated. The spin isomer (0.04 eV from the ground state) has the four oxygen atoms magnetically frustrated and the two units with identical up and down magnetic polarization. Both (4,4) and (4.6) oxides, have all bridge positions occupied by oxygen atoms. Additionally, the ferromagnetic (4,10) oxide ($8\mu_B$), with a high oxidation rate and all bridge and top positions occupied, where FeO units are more important and the Fe subcluster is broken.

Figure 14 shows the total density of states (DOS), and the partial contribution of iron atoms (cyan line) and oxygen atoms (red lines), for neutral Fe_4O_m oxides and for each oxidation rate ($m = 1 - 14$). Vertical lines indicate the Fermi level. The magnetic behavior of Fe_4O_m oxides discussed above is reflected in the DOS. The four magnetic phases are well differentiated. For $m = 1 - 3$, the strong ferromagnetic character is remarkable. The contribution of oxygen is higher at $m = 3$, although most of the contribution in this first ferromagnetic phase comes from the iron subcluster. For m=4, an antiferromagnetic state can be observed with identical up and down contributions of both iron and oxygen. At this oxidation rate, a remarkable change in density of states happens, resulting similar density

of states for n=$5-8$, with clear antiferromagnetic character. The density of states changes dramatically for $m = 9 - 10$, with oxygen atoms bound on top positions of the iron atoms, with ferromagnetic character, but where, unlike the first phase, the contribution of oxygen to the total density is much higher. For $m = 11$, the oxidation rate where oxygen starts to bind molecularly, the density of states changes, as a consequence of the antiferromagnetism of the last phase, and for m=$13-14$, the existence of highly coordinated and oxygen-saturated iron atoms is reflected.
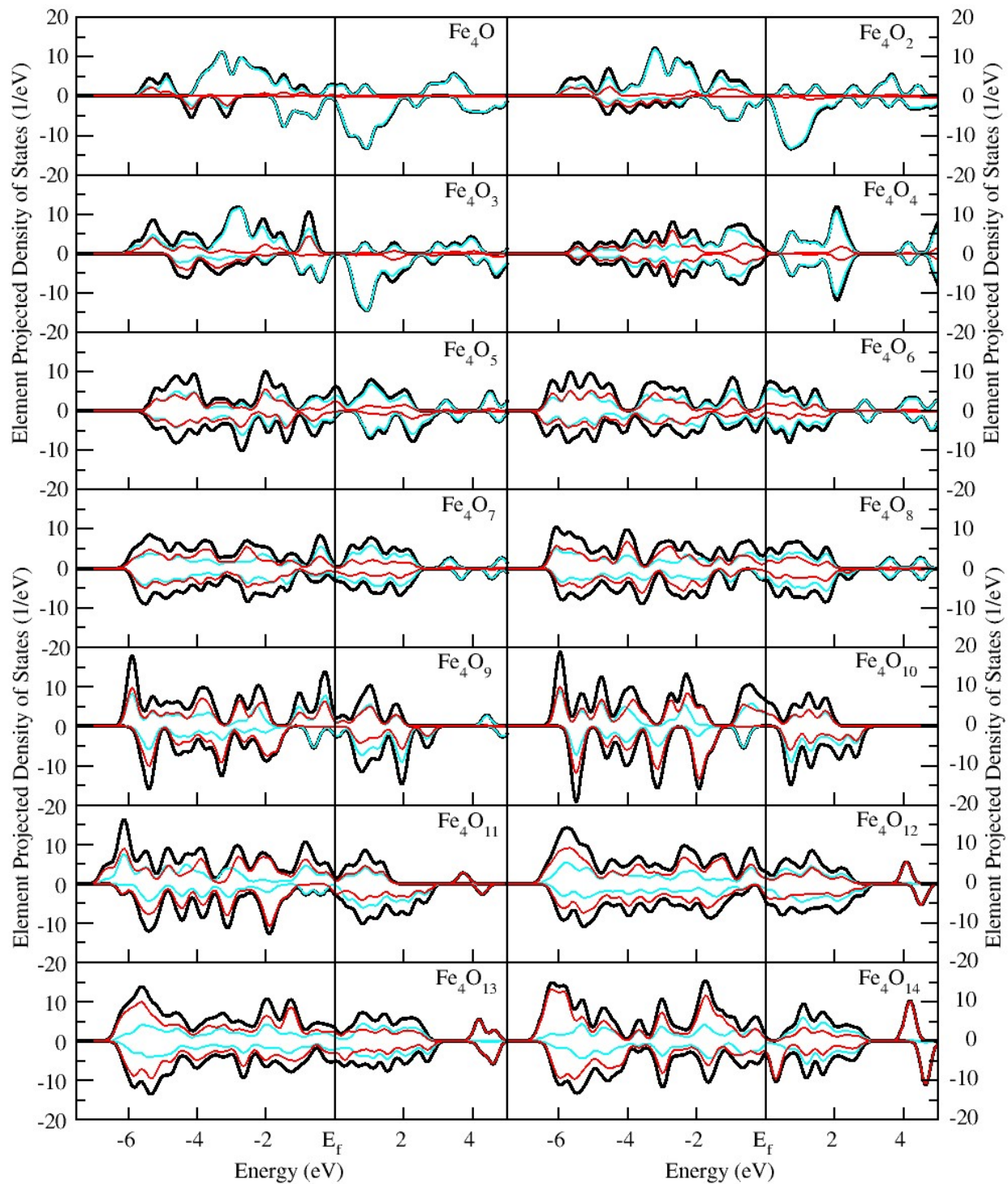
FIG. 14. (Color online) Total DOS (black line) partial contribution of iron (cyan line) and oxygen atoms (red line) of neutral Fe_4O_m ($m = 1 - 14$) oxides. The vertical line marks the Fermi energy.

3. *Iron oxides $Fe_5O_m^{0\pm}$ and $Fe_6O_m^{0\pm}$, $m = 1 - 16$*

The reentrance of the magnetic moment is also obtained for the Fe_5O_m oxides. Figure 15 shows the energy difference between spin isomers of the ground state structure (5.m.I). The first magnetic phase extends up to $m = 4$, compact iron subclusters are preserved and O atoms bind in the first bridge-hollow positions. The total magnetic moments are very high (17-19 μ_B) and ferromagnetic-like character is clearly established (see Figure 15). We highlight the (5,4) oxide with high stability (see Figures 7 and 8). The second antiferromagnetic phase, from $m = 5$ to $m = 9$ ($m = 10$ for the cationic oxide), corresponds to the cases for which all bridge positions or most of them are occupied by oxygen atoms. The reentrance of the total magnetic moment occurs at the third ferromagnetic phase, with values of 10-16 μ_B, from $m = 10$ ($m = 11$ for the cationic oxide) to $m = 15$ ($m = 14$ for the cationic oxide). Oxygen atoms bind on top positions until all them are occupied at $m = 13$, where the magnetic solution is clearly obtained (Figure 15). The last antiferromagnetic phase can be observed at $m = 16$, with two bound oxygen molecules. In addition to the influence of the charge in the limits between different regions, a lower total magnetic moment for the cation is found at $m = 13$. Also, for the anion with $m = 11$ the total magnetic moment is small as a consequence of the structural change that takes place due to the charge difference.
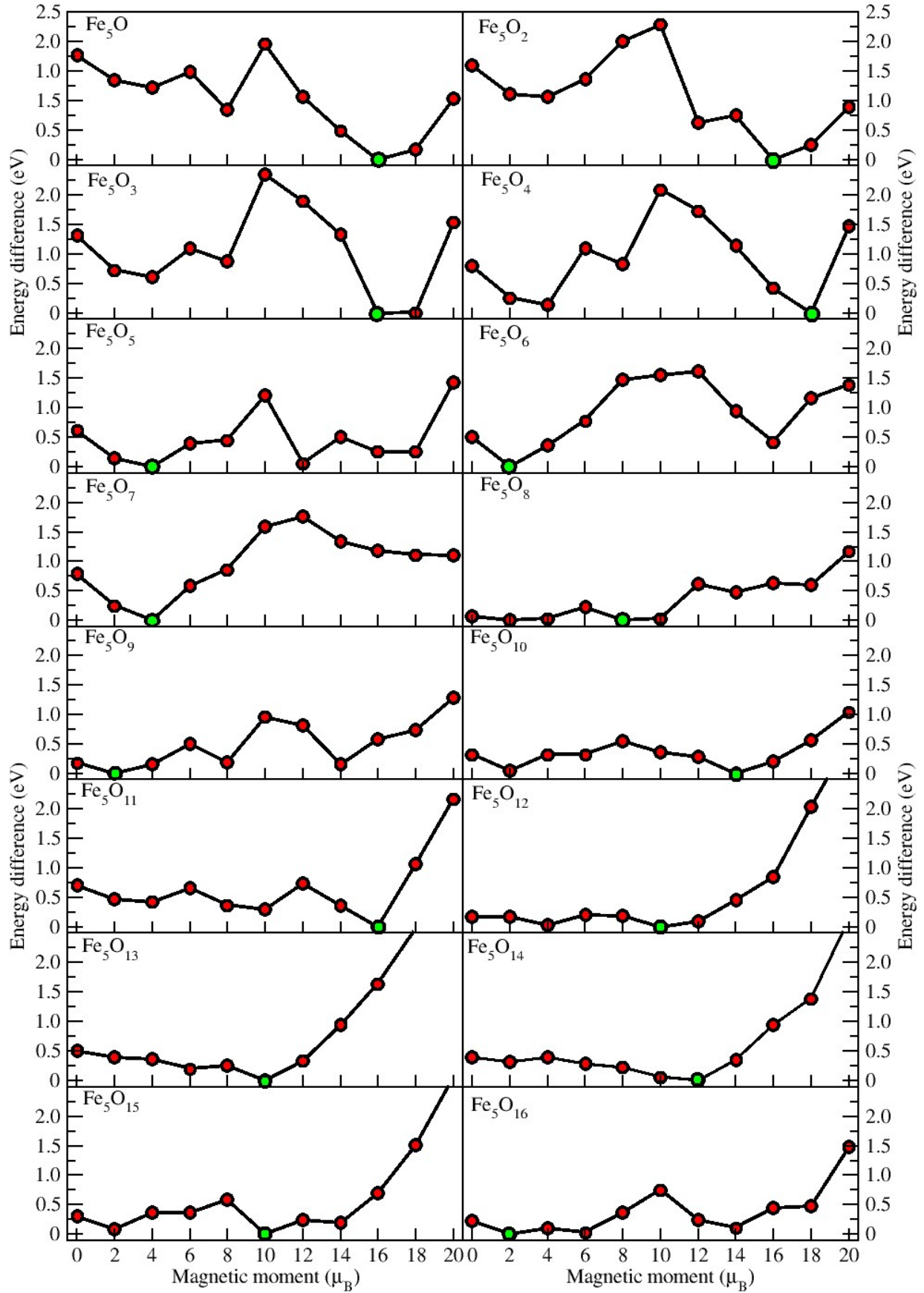
FIG. 15. (Color online) Energy difference between the spin isomers and the ground state solution (green circle, 5.m-I structure) as a function of the total magnetic moment for neutral Fe_5O_m

Therefore, for $n = 5$, we highlight four clusters due to their high stability, with different magnetic behaviour: the ferromagnetic (5,4) oxide (first magnetic phase, $\mu = 18\mu_B$), the antiferromagnetic (5,6) hexahedral-like structure with six bridging oxygens and (5,8) pyramid-like structure with all bridge occupied by oxygen (second magnetic phase $\mu = 2\mu_B$), and the ferromagnetic (5,13) pyramid-like structure with oxygen atoms occupying all bridge and top positions (third magnetic phase, $\mu = 10\mu_B$).

As for the other sizes, the reentrance of the magnetic moment also takes place for $n = 6$ and $m = 15$ with all bridge and top positions, of an already open triangular prism, occupied by oxygen atoms (for cationic oxide the ferromagnetic isomer is at 0.03 eV with 7 μ_B). Then, when the first oxygen molecule bind to an iron atom, only the cationic oxide keeps a high total moment, while the neutral and anionic oxides become again antiferromagnetic.

It is worth noting that the study of spin isomers, and what is more, the study of the possible magnetic configurations, in each of the atoms, is fundamental in this type of DFT calculation. In this way, structures such as 6.7-I and 6.8-I are obtained, where the initial magnetic configuration is crucial in the resulting geometry, which reflects the important relationship between magnetic and geometric arrangement.

IV. CONCLUSIONS

The connection between the structural patterns and magnetic properties of $Fe_nO_m^{0/\pm}$ ($n = 1 - 6$) oxide clusters has been investigated by means of DFT-GGA calculations that, allowed us to compare the fragmentation channels of cationic oxides with experimental results so us to confirm plausible geometrical arrangements. The ground state structures have been obtained by testing a large number of initial geometries and different oxygen environments and optimizing them by means of conjugate gradients. Those initial geometries were constructed i) as planar and three dimensional arrangements of FeO units; ii) as small pure iron clusters covered with consecutive oxygen atoms and molecular oxygen absorption for the highest oxidation rates; iii) with the help of the Fukui functions to locate the most nucleophilic regions to be covered by oxygen. A rich map of structural and spin isomers is found, for each of states of charge, once a detailed computational study have been done taking into account different spin isomers, with ferromagnetic and antiferromagnetic-like arrangements for each of geometric isomers with different oxygen environments. For $n =$

1, results are in agreement with previous calculations, resulting a decrease of magnetic moment of the iron atom upon addition of oxygen, with an important effect of the added or subtracted charge. For $n = 2 - 3$ the ground state structures are planar and, specially at low oxidation rates, charge has also an important influence. For $n = 4 - 6$ the ground state structures are three dimensional (3D) with tetrahedral ($n = 4$), pyramidal and hexahedral ($n = 5$), decahedral, octahedral-like ($n = 6$) and zincblenda-like geometries as the cluster size increases.

Due to the strong iron-oxygen bonding, there is a clear tendency to maximize the number of iron-oxygen bonds and as consequence of the electronic transfer from iron to oxygen atoms, an uniform oxygen distribution is found. Oxygen atoms preferably occupy bridge or hollow sites, and when all sites are saturated, they tend to bond on top positions. Further oxidation takes place through molecular adsorption. As the oxygen content increases, the iron-iron bond weakens, due to the charge transfer from iron to oxygen, what is reflected in the increasing Fe-Fe bond length. Consequently, from a certain size there is no longer an iron subcluster surrounded by oxygen, and FeO units become more preponderant. This fact is reflected on minimum values of FeO distances when all bridge and top positions are occupied. The binding energy increases faster at low oxidation rates, and then it presents relative maxima when all bridge, or most of them, are occupied by oxygen atoms and when all bridge and top positions are occupied. Once the molecular adsorption takes place, FeO distances increase, being at the same time very high the Fe-Fe distances, and thus the binding energy decreases. For cationic oxides, the fragmentation channels of these clusters are obtained and compared with experimental measurements of photofragmentation, reproducing the main features of experiments and providing support to our calculated structural geometries and energetic stabilities.

Interrelated effects between geometrical structures, oxygen environment, magnetism and stability of iron oxides, with an important effect of the charge, specially on the stability, result in the finding of very stable antiferromagnetic (with more open iron subclusters), and very stable ferromagnetic iron oxide nanoparticles (with a broken iron subcluster), both with high oxidation states. The total magnetic moment of iron oxides reflects the couplings between local magnetic moments of different sites. Iron atoms preserve their high local magnetic moment as long as the oxidation rate is low. When the oxygen content increases, and all or almost all bridge sites are occupied, the iron couplings have an antiferromagnetic

character. At the oxidation rate at which oxygen atoms start to bind on top positions results in a small energy difference between ferromagnetic-like and antiferromagnetic-like spin isomers. Moreover, local magnetic moments of iron atoms with oxygen bound on top, strongly decreases. When almost all or all top positions are occupied by oxygen, the local moments of iron atoms are about 1.4 μ_B, but couplings become again parallel and, surprisingly, oxide clusters with high oxidation rates and with high magnetic moments are found. Finally, at very high oxidation rates, oxygen molecules cause the iron oxides to become antiferromagnetic, and the binding energy to decrease. The effect of the charge excess of defect on the magnetic properties becomes more important at those oxidation rates between two ferromagnetic-antiferromagnetic phases.

Positive peaks in the second energy difference match the position of binding energy maxima. When all bridge or most of them are occupied, maxima correspond to clear antiferromagnetic oxide clusters, whereas when all bridge and top positions are occupied, maxima correspond to clear magnetic ones. This means that, despite the high degree of oxidation, certain oxided clusters which are very stable retain a high magnetic moment. We have found a reentrance of magnetic moment never before reported before for iron oxide clusters, to our knowledge. We have identified certain oxides $(4, 10)^{0/\pm}$, $(5, 13)^{0/-}$ and $(6, 15)^{0/-}$ with parallel couplings and a considerable large total magnetic moment, as well as a high relative stability, an interesting result in the context of magnetic grains design. These magnetic properties and the biocompatibility of iron oxide nanoparticles with high binding energy, might be interesting also in nanomedicine. The large moment of these magnetic grains is due to the promotion of parallel magnetic couplings, despite their significant oxidation rate, an unavoidable fact in environmental conditions.

---

* begonia@ubu.es

[1] Bao Y, Wen T, Samia A C S, Khandhar A, Krishnan M (2016) Magnetic nanoparticles: material engineering and emerging applications in lithography and biomedicine. J Mater Sci 51:513-553

[2] Xie J, Huang J, Li X, Sun S, Chen X (2009) Iron oxide nanoparticle platform for biomedical applications. Curr Med Chem 16:1278-1294

[3] Namdeo M, Saxena S, Tankhiwale R, Bajpai M, Mohan YM, Bajpai SK (2008) Magnetic nanoparticles for drug delivery applications. J Nanosci Nanotechnol 8:3247-3271

[4] Gazeau F, Levy M, Wilhelm C (2008) Optimizing magnetic nanoparticle design for nanother-motherapy. Nanomedicine 3:831-844

[5] Reimer P, Balzer T (2003) Ferucarbotran (Resovist): a new clinically approved RES-specific contrast agent for contrast-enhanced MRI of the liver: properties, clinical development, and applications. Eur Radiol 13:1266-1276

[6] Krishnan KM (2010) Biomedical nanomagnetics: a spin through possibilities in imaging, diagnostics, and therapy. IEEE Trans Magn 46:2523-2558

[7] Huijuan You, Wenting Shang, Xiangde Min1, Jeffrey Weinreb, Qiubai Li, Michael Leapman, Liang Wang, and Jie Tian, Science Advances 2020, 6, DOI: 10.1126/sciadv.aax6040

[8] Hongbin Wu, Sunil R. Desai and Lai-Sheng Wang, J. Am. Chem. Soc. 1996, 118, 5296-5301

[9] Lai-Sheng Wang, Hongbin Wu, and Sunil R. Desai, Phys. Rev. Lett. 1996, 76, 4853-4856

[10] James B. Griffin and P. B. Armentrout, J. Chem. Phys 1997, 107, 5345-5355

[11] James B. Griffin and P. B. Armentrout, J. Chem. Phys 1997, 106, 4448-4462

[12] Detlef Schroder, Phillip Jackson and Helmut Schwarz, J. Inorg. Chem 2000, 2000, 117-1175

[13] K. S. Molek, C. Anfuso-Cleaty, and M. A. Duncan, J. Phys. Chem. A 2008, 112, 9238-9247 2000, 117-1175

[14] Ming Li, Shu-Rong Liu, and P. B. Armentrout, J. Chem. Phys 2009, 131, 144310

[15] H. Shiroishi, T. Oda, I. Hamada, and N. Fujima, Eur. Phys. J. D., 2003, 24, 85-88

[16] H. Shiroishi, T. Oda, I. Hamada, and N. Fujima, Polyhedron, 2005, 24, 2472-2476

[17] A. Erlebach, C. Hühn, R. Jana and M. Sierka, P.C.C.P., 2014, 16, 26421-26426

[18] Meng Ju, Jian Lv, Xiao-Yu Kuang, Li-Ping Ding, Cheng Lu, Jing-Jing Wang, Yuan-Yuan Jin, and George Maroulis, RSC Adc. 2015, 5, 6560-6570

[19] Nelly M. Reilly, J. Ulises Reveles, Grant E. Johnson, Jorge M. del Campo, Shiv N. Khanna, Andreas M. Ko1ster, and A. W. Castleman, Jr. J. Phys. Chem. C 2007, 111, 19086-19097

[20] Nelly M. Reilly, J. Ulises Reveles, Grant E. Johnson, Shiv N. Khanna, and A. W. Castleman, Jr. J. Phys. Chem. A 2007, 111, 4158-4166

[21] Khhei Koyama, Satoshi Kudoh, Ken Miyajima, Fumitaka Mafune, Chem. Phys. Lett. 2015, 625, 104-109

[22] Yanbiao, Qian Chen, and Jinlan Wang, J. Nanosci. Nanotechnol. 2012, 12, 6488-6493

[23] Soumendu Datta and Badiur Rahaman, AIP ADVANCES, 2015, 5, 117231 118, 3899-3905

[24] P. Wang, M. Qiu, X. Lu, W. Jin, C. Li, G. Lefkidis and W. Hubner, Phys. Rev. B 2020, 101, 104414

[25] J. M. Soler, E. Artacho, J. D. Gale, A. García, J. Junquera, P. Ordejón, and D. Sánchez-Portal, J. Phys.: Condens. Matter 14, 2475 (2002)

[26] J. P. Perdew, K. Burke, and M. Ernzerhof, Phys. Rev. Lett. 1996, 77, 3865

[27] N. Troullier, and J.L. Martins, Phys. Rev. B 1991, 43, 1993

[28] L. Kleinman and D. M. Bylander, Phys. Rev. Lett. 1982, 48, 1425

[29] S. G. Louie, S. Froyen, and M. L. Cohen, Phys. Rev. B 1982, 26, 1738

[30] P. Fuentealba, P. PÃ©rez, R. Contreras, J. Chem.Phys. 2000, 113, 2544-2551

[31] W. Yang, R.G. Parr, Hardness, Proc. Natl. Acad. Sci. U. S. A. 1985, 82, 6723-6726

[32] P. Geerlings, F. De Proft, W. Langenaeker, Chem. Rev. 2003, 103, 1793-1873

[33] G. L. Gutsev, S. N. Khanna, B. K. Rao, and P. Jena, J. Phys. Chem. A 1999, 103, 5812

[34] Huber, K. P.; Herzberg, G. Molecular Spectra and Molecular Structure: IV. Constants of Diatomic Molecules; Van Nostrand Reinhold: New York, 1979.

[35] Lias, S. G.; Bartmess, J. E.; Leibman, J. F.; Levin, J. L.; Levin, R. D.; Mallard, W. G. J. Phy. Chem. Ref. Data 1988, 17, Suppl. No. 1.

[36] Smoes, S.; Drowart, J. High Temp. Sci. 1984, 17, 31

[37] Merer, A. J. Annu. ReV. Phys. Chem. 1989, 40, 407.

[38] Fisher, E. R.; Elkind, J. L.; Clemmer, D. E.; Georgiadis, R.; Loh, S. K.; Aristov, N.; Sunderlin, L. S.; Armentrout, P. B. J. Chem. Phys. 1990, 93, 2676.

[39] Loh, S.K.; Lian, L.; Armentrout, P. B. J. Chem. Phys. 1989, 91, 6148

[40] R. H. Aguilera-del-Toro, F. Aguilera-Granja, L. C. Balbás and A. Vega, Phys. Chem. Chem. Phys. 2017, 19, 3366.